Multi-Satellite Data Assimilation for Large-Scale Hydrological-Hydrodynamic Prediction: Proof of Concept in the Amazon Basin

Sly Wongchuig, R. Paiva, Vinícius Siqueira, F. Papa, A. Fleischmann, S. Biancamaria, A. Paris, Marie Parrens, A. Al Bitar

Multi-Satellite Data Assimilation for Large-Scale Hydrological-Hydrodynamic Prediction: Proof of Concept in the Amazon Basin

S. Wongchuig[1] , R. Paiva[2] , V. Siqueira[2] , F. Papa[1,3], A. Fleischmann[4], S. Biancamaria[1] , A. Paris[1,5], M. Parrens[6,7] , and A. Al Bitar[7]

[1]Laboratoire d'Etudes en Géophysique et Océanographie Spatiales (LEGOS), Université de Toulouse, CNES/CNRS/IRD/UT3, Toulouse, France, [2]Instituto de Pesquisas Hidráulicas IPH, Universidade Federal do Rio Grande do Sul UFRGS, Porto Alegre, Brazil, [3]Institute of Geosciences, Campus Universitario Darcy Ribeiro, Universidade de Brasília (UnB), Brasília, Brazil, [4]Instituto de Desenvolvimento Sustentável Mamirauá, Tefé, Brazil, [5]Hydro Matters, 1 Chemin de la Pousaraque, Le Faget, France, [6]Dynafor, Université de Toulouse, INRAE, INPT, INP-PURPAN, Castanet-Tolosan, France, [7]Centre d'Etudes Spatiales de la Biosphère (CESBIO), Toulouse University (CNES, CNRS, INRAe, IRD, UPS), Toulouse, France

Abstract Satellite remote sensing enhances model predictions by providing insights into terrestrial and hydrological processes. While data assimilation techniques have proven promising, there is a lack of standardized and effective approaches for integrating multiple observations simultaneously. This study presents a novel assimilation framework, the multi-observation local ensemble-Kalman-filter (MoLEnKF), designed to effectively integrate multiple variables, even at scales different than the model. Evaluation of MoLEnKF in the Amazon River basin includes assimilation experiments with remote sensing data only, including water surface elevation (WSE), terrestrial water storage (TWS), flood extent (FE), and soil moisture (SM). MoLEnKF demonstrates improvements in a scenario where regions lack in-situ hydroclimatic records and when assuming uncertainties of large-scale hydrologic-hydrodynamic models. Assimilating WSE outperforms daily discharge and water-level estimations, achieving 38% and 36% error reduction, respectively. However, the monthly evapotranspiration estimate achieves the greatest error reduction by assimilating SM with 11%. MoLEnKF always remains in second position in a ranking of error and uncertainty reduction, providing an intermediate condition, being able to holistically outperform univariate experiments. MoLEnKF also outperform state-of-the-art models in many cases. This study suggests potential improvements, urging exploration of correlations between assimilated variables and adaptive localization methods based on seasonality. The flexibility and the elegant way of expressing the LEnKF equations by MoLEnKF facilitates their application with different types of variables, compatible with large-scale hydrologic-hydrodynamic models and missions such as SWOT. Its robustness ensures easy replicability worldwide, facilitating hydrological reanalysis and improved forecasting, establishing MoLEnKF as a valuable tool for the scientific community in hydrological research.

Plain Language Summary The use of satellites to collect information from far away helps us to understand how water behaves on the continents. But combining all this data with uncertain computer models is complicated. This study introduces a new method called multi-observation local ensemble-Kalman-filter (MoLEnKF) to combine many different kinds of data at once. We tested MoLEnKF in the Amazon River basin, using satellite data on water levels, terrestrial water storage, flood extent and soil moisture. MoLEnKF by using all these observations at the same time obtained better results holistically than the individual experiments, improving our ability to predict aspects such as the amount of discharge, water level and evapotranspiration. This study is a step forward and could be really useful for understanding and predicting water-related phenomena worldwide, especially in a context of scarce or no availability of in-situ observations.

1. Introduction

Knowledge of freshwater availability and its changes is essential for water management and to support the operation of emergency plans, as well as for climate change monitoring. For instance, the estimation of river discharge and water level at various time scales is of primary importance for hydrological applications, as it aggregates all water cycle processes in the upstream drainage basin. To do so, hydrologists typically attempt to model the water cycle components with external forcing's varying in space and time, which are subject to various uncertainties (Gudmundsson et al., 2019; Milly et al., 2005; Pathiraja et al., 2016).

Over the past three decades, significant advances have been made in large scale hydrological modeling. Models are now capable to represent complex water cycle processes at continental and even global land areas (Archfield et al., 2015; Bierkens, 2015; Decharme et al., 2012; Miguez-Macho & Fan, 2012; R. C. D. de Paiva et al., 2013; Siqueira et al., 2018; Sood & Smakhtin, 2015; Yamazaki et al., 2013). In parallel, accurate observations and estimates of key hydrological variables are now available, enabling to better constrain the conceptual hydrological models and to reduce uncertainties related to model parametrization and representation of hydrologic and hydraulic characteristics (Garambois et al., 2017; Kuppel et al., 2017; Nijzink et al., 2018). However, in-situ networks, traditionally used to calibrate/validate models, and more recently to feed data assimilation (DA) techniques, remain scarce in many of the world's watersheds, especially in vast and remote areas such the Amazon basin (Fassoni-Andrade et al., 2021; Lettenmaier, 2017; Loukas & Vasiliades, 2014) or the Congo basin (Alsdorf et al., 2016; Laraque et al., 2020; Tshimanga & Hughes, 2014).

To overcome this limitation, satellite remote sensing has been long used in geophysical sciences since the launch of the Landsat-1 satellite in 1972. Remote sensors directly or indirectly measure different types of terrestrial parameters, mainly through electromagnetic radiation reflected/emitted from the Earth's surface (Schmugge et al., 2002). During the last decades, these sensors have also increased their spatial coverage, quality and spatial-temporal resolution (Fassoni-Andrade et al., 2021; Pietroniro & Prowse, 2002). Remote sensing variables, such as soil moisture, vegetation cover, surface water elevation and extent, among others, have been widely used in hydrology, as they provide fundamental information in poorly monitored regions (L. Chen & Wang, 2018; Kittel et al., 2018; Sandholt et al., 1999; Scanlon et al., 2016; Tang et al., 2009; Wagner et al., 2009). This leads to improvements in the physical representation of hydrological and hydraulic processes in models (Oliveira et al., 2021; Pietroniro & Prowse, 2002; Schneider et al., 2017; Yu, 2015). Therefore, remote sensing is suitable for global and continental hydrological applications (López et al., 2017; Melesse et al., 2007; Smith, 1997) and in large and remote regions, such as the Amazon (Fassoni-Andrade et al., 2021; Hess et al., 2015; Koblinsky et al., 1993) and the Congo basins (Alsdorf et al., 2016; Becker et al., 2018; B. Kitambo et al., 2022; Fabrice Papa et al., 2022; Paris et al., 2022).

Satellite monitoring of rivers is a current hot topic in hydrological studies (Bjerklie et al., 2023; Angelica Tarpanelli et al., 2020). However, discharge estimates from space are still limited (Angelica Tarpanelli et al., 2022) because they were not the main objective of current satellite missions, even if it will be somewhat improved with the new data from the SWOT satellite mission launched in December 2022. In addition, the current network of virtual stations from radar satellites that monitor water levels continues to have temporal and spatial limitations. For example, the long satellite repeat cycle means that the satellite may miss important hydrological events (e.g., daily or sub-daily flash floods) between revisits. Also, the low spatial resolution of the radar altimeter, represented by the antenna footprint (between 1.7 and 3 km for calm waters), limits the measurement to wide rivers only, due to interference of the returned radar signal by non-water features (Sulistioadi et al., 2015).

In this context, taking advantage of the variety of remote sensing techniques with the wider spatial and temporal distribution of hydrological models could also foster advances in forecasting (Montzka et al., 2012). In this sense, many recent initiatives integrate remote sensing data into large-scale hydrological and hydrodynamic models (Alfieri et al., 2022; L. Chen & Wang, 2018). In addition, many studies show how new types of observations are revolutionizing hydrological prediction in large-scale models (Döll et al., 2008; Kauffeldt et al., 2016; Nijzink et al., 2018; Pietroniro & Prowse, 2002; Pimentel et al., 2023; Revilla-Romero et al., 2016; Siqueira et al., 2018; Angelica Tarpanelli et al., 2022; Wanders, Karssenberg, et al., 2014).

Techniques such as DA have been developed to obtain the best estimate of the current state of a system by the optimal combination of observations and mathematical models, whereby updating of modeled state variables and possibly also other model components like parameters (Yuqiong Liu & Gupta, 2007; Moradkhani et al., 2005; Reichle, 2008; Shi et al., 2014). DA has been used for decades in numerical weather prediction and, more recently, in hydrological sciences (Andreadis et al., 2017; Lettenmaier, 2017; Nair et al., 2020; Reichle et al., 2002). In this sense, DA can contribute to improve the internal dynamics of the model and the resulting hydrological predictions (N. Tangdamrongsub et al., 2015). Specific methodologies such as the ensemble Kalman filter (EnKF) and its derivatives have been evaluated in hydrology to adequately consider the nonlinear nature of hydrological processes (Evensen, 1994; Fossum & Mannseth, 2017; Houtekamer & Mitchell, 2006; Paiva et al., 2013; Reichle et al., 2002; Wongchuig et al., 2019). As a consequence, many large-scale hydrological models and DA schemes have been used to improve their estimates of state variables (and possible parameters

e.g., Brandhorst & Neuweiler, 2023; Camporese & Girotto, 2022; Moradkhani et al., 2005; Panzeri et al., 2013) using remotely sensed observations, such as soil moisture (Baguis & Roulin, 2017; Blyverket et al., 2019; Corato et al., 2014; W. T. Crow & Ryu, 2008; Wade T. Crow & Wood, 2003; Lievens, Reichle, et al., 2017; Massari et al., 2015; Visweshwaran et al., 2024), surface brightness temperature (De Lannoy & Reichle, 2016; Lievens, Martens, et al., 2017; X. Tian et al., 2010), evapotranspiration (Zou et al., 2017), terrestrial water storage variation (Khaki et al., 2017, 2018, 2019; Shokri et al., 2018), flood extent (Lai et al., 2014), radar altimetry (Andreadis et al., 2007; Michailovsky et al., 2013; Paiva et al., 2013; Schneider et al., 2018), among others. While most of them have used one single type of variable (e.g., Musuuza et al., 2020; Tangdamrongsub et al., 2020), recent studies have shown the benefits of using multiple types of information at the same time, which constrains the model state variables to be more physically representative (Brocca et al., 2012; L. Chen & Wang, 2018; Khaki et al., 2020; S. V. Kumar et al., 2015; De Lannoy & Reichle, 2016; Haksu Lee et al., 2011; Nijzink et al., 2018; Su et al., 2014; Trudel et al., 2014; Wanders, Bierkens, et al., 2014). For instance, particular experiments of assimilating soil moisture (SM) and streamflow (Abbaszadeh et al., 2020; García-Alén et al., 2023; Visweshwaran et al., 2024; Yan & Moradkhani, 2016), SM and evapotranspiration (Gavahi et al., 2020, 2022), SM and leaf area index (W. Wang et al., 2024) reduced errors in the prediction of model variables compared to when only one observation was assimilated. However, no exhaustive and simple bootstrap procedures combining multiple observations at different scales in a DA scheme have been described so far, especially for hydrologic-hydrodynamic models, which may be of great interest for future research in this field. This approach was referred to by Montzka et al. (2012) as multivariate multiscale DA, which refers to the simultaneous assimilation of observational data from multiple model state variables and whose observations may or may not be obtained at a resolution significantly different from the model resolution, thus requiring the application of a scaling technique.

Since remote sensing data are usually available globally and many regions still lack in-situ data to perform calibration and/or validation of hydrologic-hydrodynamic models, the following scientific questions arise. Is it possible for DA techniques using only remotely sensed observations to achieve performance levels similar to those of reference models (e.g., calibrated models) for hydrological and hydraulic variables? (e.g., discharge, water level, evapotranspiration, among others)? How much is the improvement in performance and uncertainty when using DA from single observations and what is the added value of using multiple observations?

In this context, in this study we take advantage of the large number and variety of remote sensing data available since the last decades that already proved to be extremely useful in combination with hydrologic-hydrodynamic models, to address the following objectives: (a) to develop a straightforward technical basis for the assimilation of multiple and multiscale remote sensing information into a large-scale hydrologic and hydrodynamic model, taking into account the uncertainties of large-scale hydrologic-hydrodynamic models, which is where remote sensing observations at different spatial scales would normally be used; (b) to estimate the sensitivity in the improvement of discharge, water level and evapotranspiration through the assimilation of single and multiple remote sensing-only products as proof of concept. This approach subscribes in an important context in regions where in-situ data are scarce or non-existent to be used for calibration, validation and/or assimilation. For this application, the Amazon River basin (ARB) is used as a case study. This is the world's largest river basin with global significance for the water cycle and climate with strong hydrological signatures, where remote sensing observations have played an important role in the characterization of its hydrological processes (Fassoni-Andrade et al., 2021).

2. Material and Methods

2.1. Study Area

The ARB (Figure 1) drains around 6 million km^2 among eight countries and discharges ~20% of the freshwater that reaches the world's oceans annually, with average river discharge of 206,000 m^3 s^{-1}. However, the existing in-situ observation network remains sparse (Jose A. Marengo, 2005; Molinier et al., 1996; Willmott et al., 1994). The basins' water resources meet many human needs, such as fluvial transportation, agriculture, fisheries and energy production. Answering these needs is increasingly challenging considering the major ongoing environmental changes, especially the hydroclimate ones (Barichivich et al., 2018; Espinoza, Ronchail, et al., 2019; Ayan S. Fleischmann et al., 2023; J. A. Marengo & Espinoza, 2016; Jose A. Marengo et al., 2013; X. Y. Wang et al., 2018). Consequently, there has been an increase in the frequency of extreme hydrological events in recent
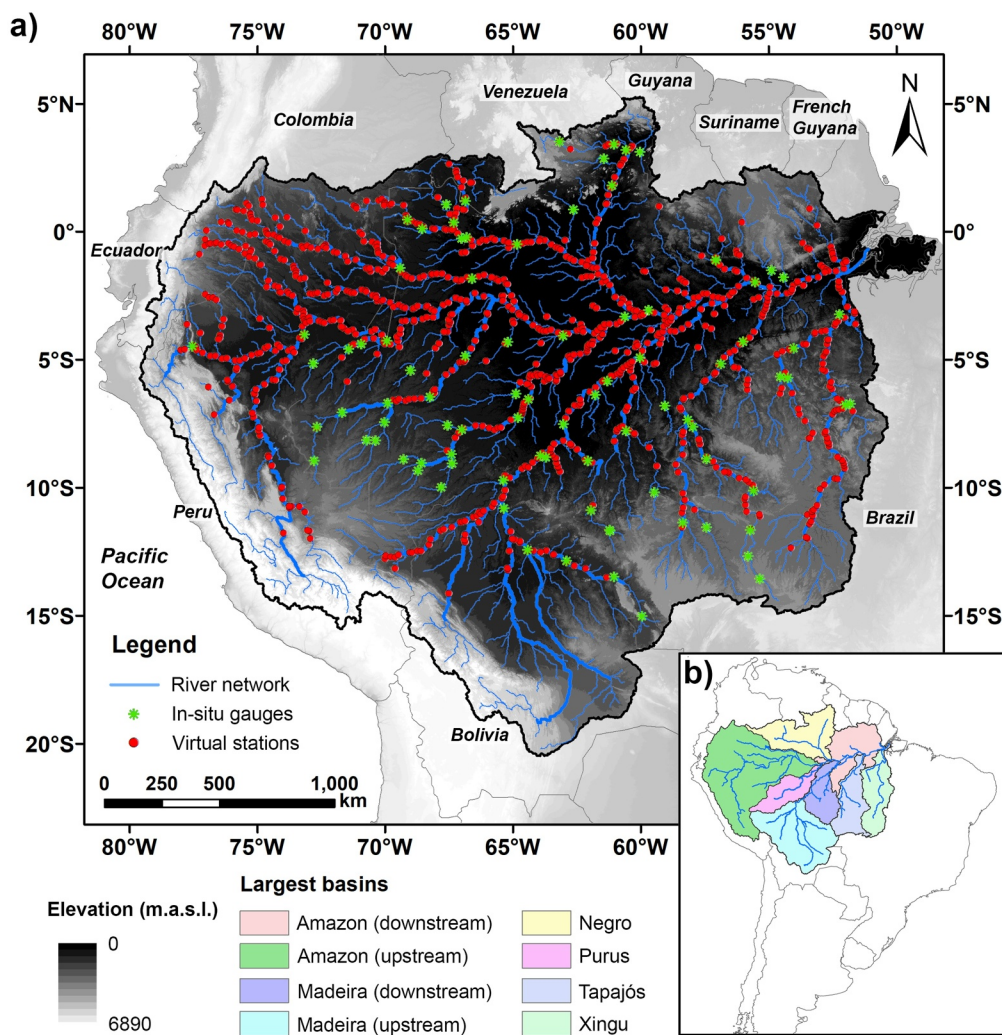
Figure 1. (a) The Amazon River Basin limit, its river network, relief map from SRTM DEM, and the in-situ discharge and water level gauging stations (green asterisk) used for validation in this study. The satellite virtual stations for rivers with widths larger than 250 m (red circles) used for assimilation are also presented. (b) The eight large sub-basins of the Amazon adopted in this study.

decades (Espinoza et al., 2009, 2011; Gloor et al., 2013; Jose A. Marengo et al., 2013), which is projected to worsen in the next decades (Boisier et al., 2015; Brêda et al., 2022; Guimberteau et al., 2013; Sorribas et al., 2016).

In this study, the ARB has been subdivided into the eight large sub-basins where observed hydrological variables are aggregated (e.g., terrestrial water storage and flood extent) for the purpose of the implementation of the DA scheme. Figure 1 shows the spatial distribution of in-situ (see Section 2.4) and satellite altimetry virtual stations (see Section 2.3.1) that provide river discharge and water level information across the ARB.

2.2. The MGB Hydrologic-Hydrodynamic Model

In this research we use the large-scale hydrologic-hydrodynamic MGB ("Modelo de Grandes Bacias" in Portuguese, an acronym meaning "Large Basins Model" model) (Collischonn et al., 2007). The MGB model was selected due to (a) its satisfactory performance for large-scale applications (R. C. D. de Paiva et al., 2013; Pontes et al., 2017; Siqueira et al., 2018); (b) successful applications in DA (Paiva et al., 2013; Wongchuig et al., 2019; Wongchuig, Cauduro Dias de Paiva, et al., 2020), which demonstrated the potential of this methodology to
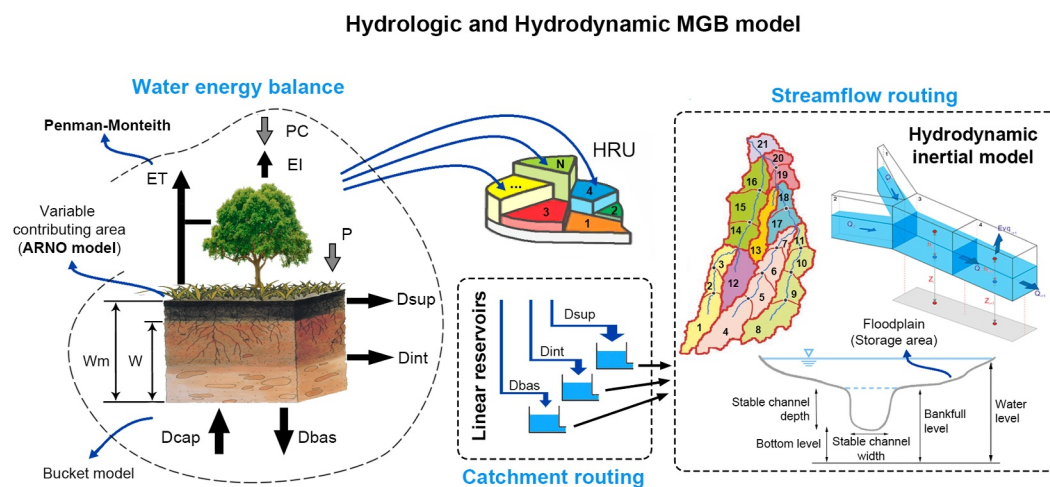
Figure 2. Schematic of the general structure of the MGB hydrologic-hydrodynamic model.

improve spatiotemporal estimates of hydraulic variables; and (c) flexibility to adapt the code for the assimilation of different observations in the local ensemble Kalman filter (LEnKF) schema used in this study Wongchuig, Cauduro Dias de Paiva, et al. (2020).

MGB is a semi-distributed hydrologic and hydrodynamic model which uses physical and conceptual based equations to simulate the continental phase of the hydrological cycle (Collischonn et al., 2007; Pontes et al., 2017). Figure 2 shows the main structure of MGB, where the watershed is discretized into non-regular unit-catchments and, in addition, into hydrological response units (HRUs), where vertical water and energy budgets are computed individually. The main hydrological soil parameters of the model are related to the saturation excess concept based on the variable contributing area concept of the ARNO model (Todini, 1996). The surface, sub-surface and groundwater runoff produced at each unit-catchment into the hydrologic module are routed to the stream network based on a linear reservoir concept. For the hydrodynamic component, each unit-catchment is composed by a river reach that includes both channel and floodplain units, the latter depicted as a simple storage with ineffective flow (Pontes et al., 2017; Siqueira et al., 2018). The flow routing in river channels is computed using the local inertial method (Bates et al., 2010; Pontes et al., 2017). This is an explicit finite difference approximation of the full 1D Saint-Venant equations by neglecting the convective acceleration term from the momentum equation. It is then able to represent complex physical processes occurring in the lower Amazon basin such as backwater effects, floodplain attenuation and flood wave transport along rivers in both 1D and 2D dimensions (Getirana et al., 2017; Yamazaki et al., 2013). For detailed information on the hydraulic channel-floodplain computation and the general configuration of the model see Supporting Information S1, Pontes et al. (2017) and Siqueira et al. (2018).

2.3. Assimilated Hydrological Variables

The following hydrologic-hydraulic variables have been considered for use in the DA scheme of the present study: water surface elevation (also called water level), terrestrial water storage, flood extent and soil moisture (Table 1 and Figure 3). The description of the data sets used for each one in the assimilation approach is provided in the next sub-sections.

2.3.1. Water Surface Elevation From Radar Altimetry

Satellite altimetry takes advantage of the reflective properties of water bodies, thus a nadir altimeter on board a satellite measures the bidirectional travel time of the pulse since it is emitted by the antenna, reflected by the surface and captured again by the sensor (CNES, 1996; Fassoni-Andrade et al., 2021; Stammer & Cazenave, 2017). Radar altimeters such as TOPEX/Poseidon (1992–2005) were initially designed to be used on relatively regular surfaces such as the oceans. Therefore, this was replaced by Jason-1 (2001–2013) and Jason-2

Table 1
Summary of the Data Sets Used in This Study for Assimilation

Data set	Data availability	Spatial resolution	Temporal resolution	Main reference	Assimilated variable	Assimilation time scale	Assimilation spatial scale	Uncertainty/ Reference
Radar altimetry:								
Jason-1	2001/12–2013/07	-	9.9 days	Asadzadeh Jarihani et al. (2013)	Water level anomaly	10–35 days	Virtual station on the drainage network	30 cm Silva et al. (2010)
Jason-2	2008/06 - 2019	-	9.9 days					
Jason-3	2016/01 - current							
ENVISAT	2002/03–2012/04	-	35 days	Frappart et al. (2006)				
Sentinel-3 A/3B	2016/02, 2018/04 - current		27 days	B. Kitambo et al. (2022)				
Terrestrial water storage:								
GRACE RL06v4	2002/04–2017/10	~1°	Monthly	Scanlon et al. (2016)	Terrestrial water storage anomaly	Interpolated to 5 days	Average in large sub-basins	11.3 mm Landerer and Swenson (2012)
GRACE-FO RL06v4	2018/05 - current							
Flood extent:								
GIEMS-2	1992–2015	~25 km	Monthly	C. Prigent et al. (2020)	Flood extent standard anomaly	Interpolated to 7 days	Accumulated in large sub-basins	15% C. Prigent et al. (2020)
Soil moisture:								
SMOS RZSM L4	2010–2020	~25 km	Daily	Al Bitar et al. (2013a)	Rescaled soil moisture	Daily	Weighted average in calibrated sub-basins	20% Al Bitar et al. (2013b)

(2008-present) and recently by Jason-3 (2016-present), ENVISAT (2002–2012) and Sentinel-3A/B (2016-present). Many of these nadir altimetry sensors that measure water surface levels have been widely used in hydrological studies (Paiva et al., 2013; Sulistioadi et al., 2015). Within the field of altimetry applied to hydrology, the term "virtual station" (VS) has been used, that is, the location of the intersection between a monitored water body (e.g., rivers, lakes, reservoirs, among others) and the satellite track (Benveniste et al., 2017; Cretaux et al., 2023). In recent years, different studies have addressed the use of altimetry VS's in hydrological applications (Frappart et al., 2012, p. 202; Leon et al., 2006; Paris et al., 2016; Roux et al., 2008). In parallel, large radar altimetry databases were developed in continental water bodies (e.g., wide rivers, lakes, reservoirs) by various research groups (Fassoni-Andrade et al., 2021; Fabrice Papa et al., 2022). In this study we use data from the Jason-1/2, ENVISAT and Sentinel 3 A/B missions corresponding to 954 VSs (see Figure 1a) spread along rivers wider than ~250 m, which were previously processed for the ARB.

2.3.2. Terrestrial Water Storage

The GRACE (Gravity Recovery and Climate Experiment) mission was developed by the U.S. space agency National Aeronautics and Space Administration (NASA) in conjunction with the German space agency German Aerospace Center (DLR), with the purpose of mapping the temporal variations of the earth's gravitational field
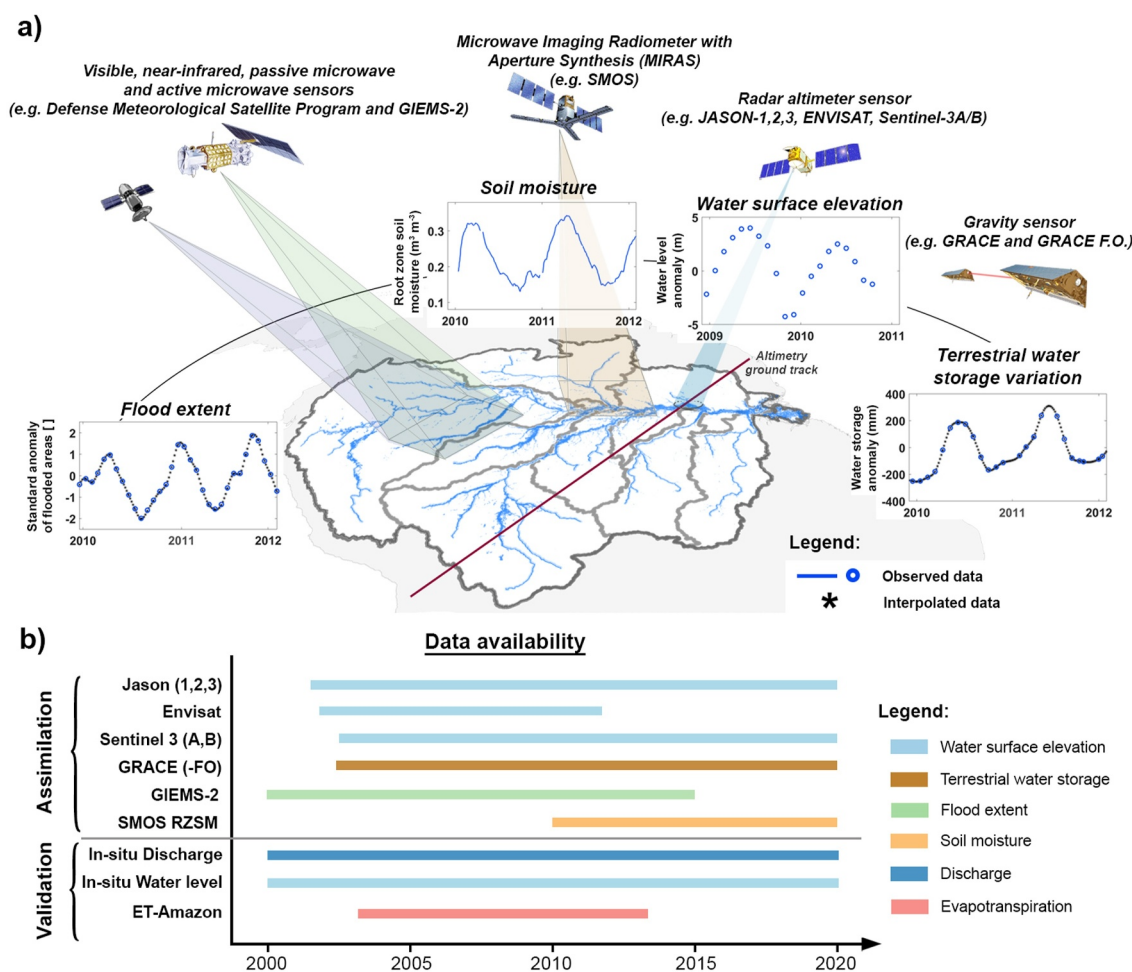
Figure 3. (a) Graphical scheme of the observational data. (b) Temporal availability of the data sets used for assimilation and validation during the period 2000–2020.

(Tapley et al., 2004). As a result, it is possible to indirectly detect the variation in terrestrial water storage (TWS) on the earth's surface in cycles of approximately 30 days, considering that water displacement on the continents is one of the main causes of mass fluctuations in the earth (Rodell & Famiglietti, 2002; Strassberg et al., 2009). The mission comprises two satellites separated by each other approximately 220 km; the variation in the Earth's gravitational field changes the distance between them, and the sensors are able to detect these variations with the sensitivity of a micrometer (Strassberg et al., 2009). Because other elements can cause a change in the gravitational field, such as atmospheric fluctuations, changes in topography, tidal effects and movements of ice or snow, the information detected by GRACE provides a series of corrections to ignore these other effects. Several studies have also shown that GRACE can be used in hydrological modeling on a large scale due to its coherent variation in water storage (Güntner, 2008; Lettenmaier & Famiglietti, 2006; Paiva et al., 2013; Ramillien et al., 2008; Reager & Famiglietti, 2009). GRACE has also contributed to the understanding of space-time variations of water storage across continents (Tapley et al., 2004). In this study, we use three products of equivalent water mass; all based on the last version (GRACE v4), but developed by different research centers and laboratories: The Jet Propulsion Laboratory (JPL), the University of Texas Center for Space Research (CSR) and the Geo-ForschungsZentrum (GFZ) Potsdam. As all three centers produced reasonably similar TWS anomalies for the period of overlap, we used an average of available estimates.

2.3.3. Flood Extent

Estimates of remotely sensed flood extent (FE) have been especially valuable in poorly monitored regions with large floodplains (Thomas et al., 2011). Different studies have shown that satellite information (e.g., Landsat, IKONOS, MODIS) through visible/infrared spectrum imagery is capable of providing adequate records of flooded areas (Brakenridge & Anderson, 2006; Y. Wang, 2004), such as GSWO (Global Surface Water Occurrence (Pekel et al., 2016)), one of the latest global surface water products based on Landsat imagery between 1984 and 2021. However, products based on visible/infrared imagery have some deficiencies in regions covered by forests and clouds (Aires et al., 2018; Ayan Santos Fleischmann et al., 2022; Smith, 1997). To overcome this limitation, active sensors in the microwave spectrum (e.g., SAR) have been used to detect flooded areas in these conditions, by measuring the backscattering index (Brivio et al., 2002; Townsend, 2002). Among them are RADARSAT-1, Sentinel 1 (Pham-Duc et al., 2017), JERS-1 (Hess et al., 2015; Å. Rosenqvist et al., 2002), ALOS PALSAR (A. Rosenqvist et al., 2004), the latter evaluated in large tropical basins such as the Amazon and Congo (Arnesen et al., 2013; Hyongki Lee et al., 2014). On the other hand, it is challenging to establish adequate methodologies to determine the extent of flooded areas and to automate the classification processes from SAR images (Brisco et al., 2009; Westerhoff et al., 2013; White et al., 2014). This would make it difficult, for example, to preprocess flood zones from these products for use in DA schemes.

In the context of combining several types of sensors that can take advantage of each other's advantages, the GIEMS (Global Inundation Extent from Multi-Satellites) database has been developed. GIEMS provides global monthly average information on flood extent through the combination of satellite observations in the visible, near infrared and passive/active microwave spectrum (F. Papa et al., 2010; C. Prigent et al., 2012; Catherine Prigent et al., 2007), and has been assessed in regional applications to estimate variations in surface and subsurface water storage across the globe (B. M. Kitambo et al., 2023; Fabrice Papa et al., 2015). FE estimates from remote sensing have been previously used for validation of the MGB model (R. C. D. de Paiva et al., 2013), although not yet for DA processes. In this study we use the GIEMS-2 data set, which provides monthly estimates of flood extent, including open water, wetlands, and floodplains. It is based on the Special Sensor Microwave/Imager and the Special Sensor Microwave Imager Sounder intercalibrated observations to produce a global data record of surface water extent from 1992 to 2015, on an equal area grid of $0.25° \times 0.25°$ at the equator (~25 km) (C. Prigent et al., 2020).

2.3.4. Soil Moisture

Active (ASCAT, Sentinel-1) and passive (SMOS, SMAP, AMSR-E) space-born microwave sensors have been used to monitor soil moisture (SM). The amount of microwave radiation that is emitted or backscattered from the Earth's surface depends on the amount of water in the soil. Wet soil emits and backscatters more microwave radiation than dry soil due to its high dielectric constant. The Soil Moisture and Ocean Salinity (SMOS) mission (Y. H. Kerr et al., 2001) is an interferometric L-Band radiometer that provides top-surface SM estimates (0–5 cm) over continental surfaces, from the inversion of multi-angular and full-polarization brightness temperatures acquired in L-Band (1.4 GHz) (Al Bitar et al., 2017; Y. Kerr et al., 2012). The use of the L-Band frequency in comparison to lower frequencies like C-Band enables to enhance the observation of soil emissions in the presence of vegetation. SMOS sensor configuration enables a 3-day revisit at the equator for ascending and descending orbits at a 40 km nominal resolution while the products are provided over 15 km L2DPGS and 25 km L3 CATDS. The Center Aval de Traitement des Données SMOS also provides a root zone soil moisture (RZSM) product (0–1 m) based on a daily frequency and at 25 km grid (Al Bitar et al., 2013a). This operational product is obtained from the assimilation of the surface SM into a sequential exponential filter with a soil properties-dependent temporal lag function. The L4 RZSM was used in this research, and it covers the period 2010–2020.

2.4. Validation Data Sets

For the validation stage, daily in-situ discharge and water level time series from 85 to 87 gauging stations, respectively, were used in this study (see Figure S1 and Table S1 in Supporting Information S1). The selection criteria was to have an upstream catchment area greater than 10,000 km^2. Around 60% and 65% of the gauging stations have more than 90% of complete data for the periods 2000–2020 and 2010–2015, respectively. The latter corresponds to the period in which the final results are presented for a fairer comparison because it is the common

period for the four assimilated variables in the multi-observation DA scheme. These data sets were provided by the Environmental Research Observatory SO HYBAM (ORE-HyBam: <http://www.orehybam.org>, last access in October 2023) and the Brazilian National Water and Sanitation Agency (ANA). To validate the actual evapotranspiration variable, the monthly ET-Amazon data set (Paca et al., 2019) was used. ET-Amazon is based on the merging of six global evapotranspiration products (GLEAM, SEBS, ALEXI, CMRSET, MOD16, and SSEBop), that are based on models and remote sensing techniques. ET-Amazon was validated with seven flux towers (see Table S2 and Figure S2 in Supporting Information S1) from the Large-Scale Biosphere-Atmosphere Experiment in the Amazon (LBA; Saleska et al., 2013). It provides monthly evapotranspiration estimates with a spatial resolution of 250 m for a 10-year period (2003–2013) and were averaged in this study over the Amazon large sub-basins (see Figure 1b) for validation purposes.

More detailed information about the in-situ gauges and data quality control used in this study can be found in the Supporting Information S1.

2.5. Methodology

2.5.1. Data Assimilation Scheme

The ensemble Kalman filter (EnKF) data assimilation method (Burgers et al., 1998; Evensen, 1994) has become popular in Earth Sciences due to its relatively simple conceptual formulation and sequential implementation (Evensen, 2003, 2004). The EnKF method uses an ensemble of state variables to sample model errors and compute the covariance error matrix that is combined with the observation error to estimate the Kalman gain. For this purpose, it is usual to estimate these errors from the perturbation of the forcing or model parameters (Biancamaria et al., 2011; Y. Liu et al., 2012; Paiva et al., 2013). Among the EnKF-based methods, the local ensemble Kalman filter (LEnKF) was implemented and evaluated in this study. It constrains the update of the state variables in a spatial area around the observation (Wongchuig et al., 2019). The localization technique has been an important breakthrough in EnKF-based methods. According to Zhu et al. (2011), it is important to screen updates that are due to spurious correlations between the observation and the model unit influenced by DA for two reasons: (a) to limit the number of ensemble members (mostly to avoid large computational effort) and (b) to disregard highly distant or physically disconnected points or regions, which could generate an artificial impact in large regions such as the ARB.

The main goal of LEnKF is to optimize the variance of model errors based on model and observation uncertainties to provide a better estimate of the model state variable. The LEnKF can be divided into two steps: forecasting and updating. As denoted by Paiva et al. (2013), the model representing the dynamics of the simulated system can be shown in a discrete form by the process equation:

$$x_{k+1} = M(x_k, u_k, \theta) + q_k \tag{1}$$

where the vector x represents model state variables, u is the model forcing, θ is the model parameters; M is the model function that relates state variables at time k with those at time $(k + 1)$; and q_k represents the model uncertainties.

The observation equation is:

$$y_k = H(x_k) + \varepsilon_k \tag{2}$$

where y_k is a vector with observations at time k (here, observed discharge or water level), H is a function that relates the model state variables x^f to its corresponding observation (y) and ε_k means the observation uncertainty.

In the stochastic formulation of LEnKF, the matrix of the background ensemble of model states x^f, is represented for each step time as:

$$x^f = \left(x_1^f, x_2^f, \ldots, x_{N_{ens}}^f\right) \tag{3}$$

where x_i^f represents each ensemble member (i) of the model states until the total number of defined members, also called realizations (N_{ens}).

The analysis x^a is estimated by the EnKF as follows:

$$x^a = x^f + K_e \left(y - Hx^f \right) \tag{4}$$

$$K_e = \rho \times \left(P_e^f H^T \right) \left[\rho_o \times \left(HP_e^f H^T \right) + R_e \right]^{-1} \tag{5}$$

where x^a is the estimated model state, K_e the Kalman Gain, P_e^f and R_e covariance matrices of model (q) and observation (ε) errors, respectively. The $(y - Hx^f)$ expression is also called innovation matrix. The ρ and ρ_o are correlation matrices in the localization scheme, and $\times$ represents the Schur product. The correlation matrices for the localization method in the assimilation of observations located in the drainage network (e.g., discharge, water level, among others) were calculated using a fifth-order function (Gaspari & Cohn, 1999) already evaluated in MGB in previous studies (Wongchuig et al., 2019; Wongchuig, Cauduro Dias de Paiva, et al., 2020; Wongchuig, Fleischmann, et al., 2020).

The error covariance matrix of the model's state variables is generated by a set of members from perturbations of the model (forcing, state variables, parameters), based on a known error:

$$P^f \cong P_e^f = \frac{\left(x^f - \overline{x^f} \right) \left(x^f - \overline{x^f} \right)^T}{N_{ens} - 1} = \frac{x'^f x'^{fT}}{N_{ens} - 1} \tag{6}$$

where the mean of the ensemble, $\overline{x^f}$, denotes the best guess and x'^f represents the ensemble of perturbations.

Considering observations, the error covariance matrix is estimated as follows:

$$y = \left(y_1, y_2, \dots, y_{N_{ens}} \right) \tag{7}$$

$$E = \left(y_1 - \overline{y}, y_2 - \overline{y}, \dots, y_{N_{ens}} - \overline{y} \right) \tag{8}$$

where y and E indicate the ensemble matrix of perturbed observations and errors due to perturbations respectively.

Therefore, the observation error covariance matrix (R_e) shown in Equation 5 is calculated as follows:

$$R_e = \frac{EE^T}{N_{ens} - 1} \tag{9}$$

Therefore, Equation 5 can be also expressed as:

$$K_e = \rho \times \left(x'^f x'^{fT} H^T \right) \left[\rho_o \times \left(Hx'^f x'^{fT} H^T \right) + EE^T \right]^{-1} \tag{10}$$

In this study the covariance matrix of the observation errors was estimated following the approach by Clark et al. (2008):

$$R_e = \left(\varepsilon_{obs} \cdot var_{obs} \right)^2 \tag{11}$$

where ε_{obs} represents the error in the observation that can be known a priori and var_{obs} indicates the value of the observed variable.

2.5.2. Multi-Satellite Assimilation and Localization Approach

The multi-satellite mission or multi-observation approach was implemented by adding complementary matrices to Hx'^f, E and $(y - Hx^f)$ arrangements, which are shown in Equation 13, by assuming n different types of

observations, that is, water level anomaly, terrestrial water storage, flood extent, soil moisture, among others. Therefore, the aforementioned matrices have dimensions $nobsT \times nens$, $nobsT \times nobsT$ and $nobsT \times nens$, respectively, and they follow the subsequent scheme:

$$nobsT^k = \sum_{i=1}^{n} nobs_i^k \qquad (12)$$

$$\mathbf{Hx}'^f = \begin{bmatrix} & & & \\ & & & \\ & & & \\ & & & \end{bmatrix}_{nobsT \times nens}$$

$$\mathbf{E} = \begin{bmatrix} \square & 0 & 0 & 0 & 0 & 0 & 0 & 0 \\ 0 & \square & \square & \square & \square & 0 & 0 & 0 \\ 0 & \square & \square & \square & \square & 0 & 0 & 0 \\ 0 & \square & \square & \square & \square & 0 & 0 & 0 \\ 0 & \square & \square & \square & \square & 0 & 0 & 0 \\ 0 & 0 & 0 & 0 & 0 & \square & \square & \square \\ 0 & 0 & 0 & 0 & 0 & \square & \square & \square \\ 0 & 0 & 0 & 0 & 0 & \square & \square & \square \end{bmatrix}_{nobsT \times nobsT} \qquad (13)$$

$$\left(\mathbf{y} - \mathbf{Hx^f} \right) = \begin{bmatrix} & & & \\ & & & \\ & & & \\ & & & \end{bmatrix}_{nobsT \times nens}$$

where $nobs_i$ means the number of observations of the same source i at the instant k and $\textbf{nobsT}$ means the total number of observations considering more than one source (i.e., multi-mission observations). In Equation 13, zero values mean that the observations between different types of variables are not correlated with each other, which has been assumed as a simplification in the implementation of this study. Different grayscale colors correspond to different types (sources) of observation.

For didactic purposes in this manuscript when differentiating this implementation from traditional approaches, we refer to the multi-observation assimilation in the LEnKF scheme as MoLEnKF, as well as to the experiment when all satellite observations are assimilated at the same time.

2.5.2.1. Localization Approaches

2.5.2.1.1. Influence Radius Along the River Network

In this specific localization method, the "covariance localization" method proposed by Houtekamer & Mitchell (2001) was implemented, in which the correlation coefficient decreases according to the distance between an observation in certain unit-catchment (i.e., discharge or water level) and all the assimilated unit-catchments within a radius of influence, following the drainage network (different to a Euclidean distance) as shown in the localization approach in Figure 4i. To assimilate water level from satellite altimetry, a 1,000 km radius of influence within the river network was applied as a locational approach, following the best estimates for the ARB as evaluated by Wongchuig et al. (2019) and Emery et al. (2018). The spatial distribution of the correlation coefficient when assimilating virtual stations is shown in Figure S3 in the Supporting Information S1. This
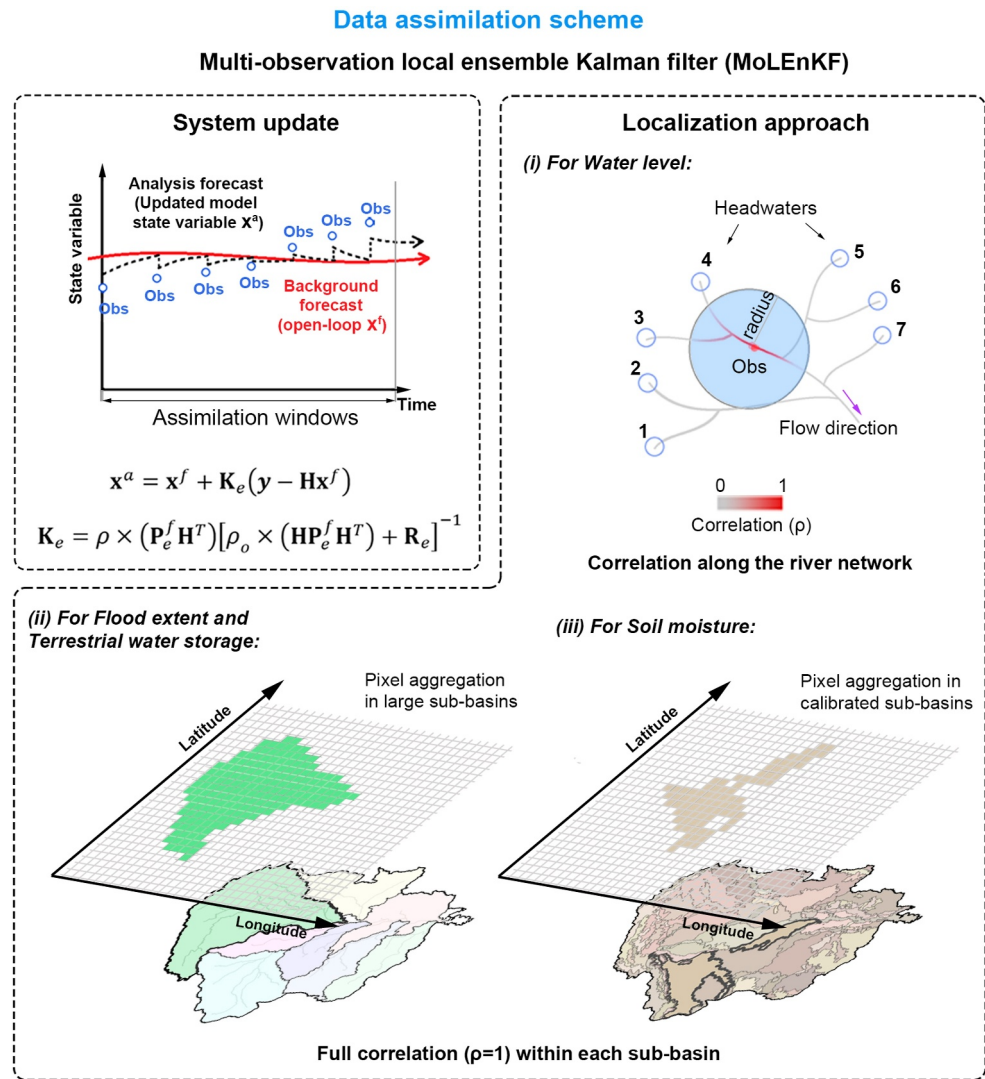
Figure 4. Schematic of the MoLEnKF data assimilation scheme and rescaling approaches (ii and iii).

Table 2
State Variables Updated in the Data Assimilation Process

State variable	Notation
Water storage in the soil surface layer	W
Water volume in the sup-surface unit catchment reservoir	VBAS
Water volume in the groundwater unit catchment reservoir	VINT
Water volume in the surface unit catchment reservoir	VSUP
Unit catchment runoff	QCEL
River discharge	Q
River water elevation	Y
Flood extent	Area
Superficial water volume	Vol
Terrestrial water storage	TWS

localization procedure updates the state variables (e.g., hydrologic and hydraulic) of the unit-catchments that have been considered (see Table 2), and within the region of influence.

2.5.2.1.2. Physical Characteristics Approach

The second localization approach within the LEnKF or MoLEnKF scheme consisted of using eight large sub-basins with similar physical characteristics (see Figure 1b). This approach is associated with the spatial rescaling of some of the observations used in this study. For the flood extent and terrestrial water storage, large sub-basins were used as a spatial limiter for the aggregation of these variables, mainly due to the coarse resolution and uncertainty of these remotely sensed data. For soil moisture, a discretization into 63 calibrated sub-basins determining each set of soil parameters was used. Finally, the localization consists of limiting the update of the state variables to the corresponding sub-basin with its own observation, as shown in Figures 4ii and 4iii.

2.5.3. Experiment Setting and Model Performance

2.5.3.1. Model Setup

The MGB model setup used in this study over the ARB is a version extracted from the configuration developed for the entire domain of South America (Siqueira et al., 2018). The ARB setup was discretized into 12,466 unit-catchments and river reaches of ∼15 km. Monthly meteorology was used for the period 1961–1990 from the Climate Research Unit (CRU) Global Climate CL 2.0 data set (New et al., 2002), which provides long-term climatology of relative humidity, surface temperature, pressure, radiation and wind speed for global land areas at 10' resolution.

2.5.3.2. Reference Model Version and Ensemble Realizations

For the evaluation of the performance of the assimilation experiments, we use as a reference the version of the MGB model based on the structure developed for South America (Siqueira et al., 2018). Since one of the objectives of this study is to quantify the performance of the DA technique in assimilating univariate and multivariate (MoLEnKF) variables in a context where large-scale models (e.g., continental, global) are used without in-situ data for calibration/validation, the authors have configured the MGB model to represent these uncertainty levels by perturbing the precipitation forcing and parameters (hydrological parameters, floodplain bathymetry and hydraulic parameters) when generating ensemble realizations. According to Wongchuig, Cauduro Dias de Paiva, et al. (2020), the uncertainty of the MGB model for discharge estimations when assuming global parameter and forcing uncertainties is about 42% for precipitation, ∼32% for hydrological parameters, ∼2% for the hydraulic parameters (depth and width of the bankfull river channel and Manning coefficient) and ∼0.51% for the floodplain bathymetry. A brief description of the main sources of uncertainty assumed for the generation of the realizations (ensemble members), which in this study 100 were realized based on the performance of this number in past studies (e.g., Paiva et al., 2013; Wongchuig et al., 2019; Wongchuig, Fleischmann, et al., 2020), is described below:

2.5.3.2.1. Precipitation

Precipitation forcing is the major source of hydrological model uncertainty (Sperna Weiland et al., 2015; Tapiador et al., 2012). The uncertainty of 22-precipitation data sets was assessed by Beck et al. (2017), which could give us an order of magnitude of the associated bias that achieves ∼17% for global data sets. Another extensive assessment of 30 global precipitation data sets (Sun et al., 2018) results for South America in values of systematic errors and random errors that ranges between 20%–40% and 60%–80% respectively for daily precipitation. Therefore, the values for systematic (β_p) and random (ε_p) errors of ∼25% and ∼70% respectively were assumed in this research as representative for the Amazon basin as documented in (Wongchuig, Cauduro Dias de Paiva, et al., 2020). These magnitudes were used to generate the perturbed precipitation based on a lognormal distribution of errors (Nijssen & Lettenmaier, 2004), and a multiplicative error as recommended by Y. Tian et al. (2013) to avoid negative values (see Equations 14 and 15). In this research we used the CHIRPS database because of its adequate representation of seasonal, interannual and long-term variability of precipitation in the Amazon (Beck et al., 2017; Espinoza, Sörensson, et al., 2019; Wongchuig et al., 2017). CHIRPS database is based on precipitation models that are merged with in-situ precipitation data (Funk et al., 2015). The latest version (CHIRPS v2.0) was used, with a spatial resolution of 0.05° and a daily time resolution.

$$P_c = \frac{1 + \beta_p}{\sqrt{\varepsilon_p{}^2 + 1}} exp\left(\sqrt{ln[\varepsilon_p{}^2 + 1]}\; s\right) P \qquad (14)$$

where P_c is the perturbed precipitation, P is the non-perturbed precipitation, ε_p is the random error (%), β_p is the systematic error, and s is a random variable that follows the time evolution of model error according to Evensen (2003):

$$S_k = \alpha S_{k-1} + \sqrt{1 - \alpha^2} w_{k-1} \quad \alpha = 1 - \frac{\Delta t}{\tau_t} \qquad (15)$$

where the coefficient $\alpha \in [0\ 1\rangle$ indicates the influence of temporal correlation on the model errors ($\alpha = 0$ indicates a high correlation, while $\alpha = 1$ indicates a random field of errors constant in time—no temporal correlation); w is a stochastic term with mean 0 and variance 1 following a Gaussian distribution; and τ_t is the temporal decorrelation length (time units). In this study we adopted $\tau_t = 10$ days following the study of Rodrigo C.D. Paiva et al. (2013) in Amazon Basin.

2.5.3.2.2. Hydrological Parameters

Most of continental and global hydrological models use parameters that are chosen based on a priori data sets without extensive calibration against in-situ discharge data (Beck et al., 2017; Siqueira et al., 2018). The uncertainty of the hydrological parameters of the model was represented by uniformly random selecting values in the range found by Siqueira et al. (2018) in the calibration of MGB model for different South American catchments (Wm = 50–2,000 mm; b = 0.01–1.6; Kbas = 0.1–4.0 mm day^{-1}, Kint = 4–40 mm day^{-1}, Cs = 1–30, Ci = 50–200 and Cb = 800–8,000 hr). Table S3 in the Supporting Information S1 describes each of these parameters in more detail.

2.5.3.2.3. Floodplain Bathymetry

Since the river bathymetry based on the DEM is central to represent adequately flooded water extent in hydrodynamic models (Bates et al., 2014), the hypsometric curve (flp) was also perturbed for each catchment, using a simple bias additive error to the floodplain elevation based on the approximation of the DEM errors. The assumed absolute bias (β_{flp}) is one of the main source of errors in global DEMs (Yamazaki et al., 2017) which is around of ~10 m. In this version of the model the floodplain bathymetry is from Baer-Earth SRTM digital elevation model (O'Loughlin et al., 2016) resampled from 3 to 15 arcsec (~90–500 m). It was adopted to account for vegetation biases in floodplains since the C-band radar used by the original SRTM is not able to penetrate fully through the canopy.

$$flp' = flp + \beta_{flp} \tag{16}$$

where β_{flp} represent the absolute bias.

2.5.3.2.4. Hydraulic Parameters

Large-scale hydrological models usually represent river bathymetry as rectangular cross sections width (w) and depth (d). These parameters could be estimated using hydraulic geometry relations as developed by Andreadis et al. (2013) in a global data set of river geometry. Uncertain river width and depth from these estimates can be modeled as:

$$w' = w * \beta_w * \varepsilon_w \tag{17}$$

$$d' = d * \beta_d * \varepsilon_d \tag{18}$$

$$n' = n * \varepsilon_n \tag{19}$$

where β and ε are regional bias and reach random errors, respectively.

The relations proposed by Andreadis et al. (2013) and Moody and Troutman (2002) present estimates ranging from approximately 1/3 to 3 at 95% confidence interval for width and 1/2.5 to 2.5 at 95% for depth which means that uncertainty could be modeled as a log-normally distributed random noise. With a multiplicative standard deviation or shape parameter (σ*) of approximately 1.73 and 1.58, which transformed to a normal σ become in 0.55 and 0.46 respectively. In addition, bias and noise show the same order of magnitude, therefore a simplification could be assumed by breaking errors as $\beta_w \sim \text{logN}(1, 1.22^2)$, $\varepsilon_w \sim \text{logN}(1, 1.22^2)$ (relative error of 39% for bias and noise) and $\beta_d \sim \text{logN}(1, 1.12^2)$, $\varepsilon_d \sim \text{logN}(1, 1.12^2)$ (relative error of 33% for bias and noise), considering total errors modeled as $\varepsilon_T = \sqrt{\beta^2 + \varepsilon^2}$ similar to proposed by Durand et al. (2016), where ε_T represents total errors. In this version of the MGB model, the river bankfull widths and depths were estimated from regional hydraulic geometry equations and a global data set (Andreadis et al., 2013).

For the Manning's coefficient, the values for natural streams (main channels and floodplain) were used as a proxy of uncertainty (Anees et al., 2017; Gichamo et al., 2012), which ranges from 0.02 to 0.16. Therefore, considering a mean of the Manning's value of ~0.056 for the main channels and floodplain, at 95% confidence interval, we can perturb it with a multiplicative noise (ε_n) that follows a lognormal distribution with a standard deviation of ~1.69, which represents approximately a relative error close to ~50%.

2.5.3.3. General Configuration of Experiments

The MGB simulations (open-loop and assimilation) were carried out between 1 January 2000 and 31 December 2020 using a daily time step; a warm up period of two years was considered to discard the influence of initial conditions. Model results of the assimilation experiments were validated in terms of daily discharge and water level against in-situ data sets, and in terms of monthly evapotranspiration against the ET-Amazon database, which is based on remote sensing products combined with flux tower observations (see Table S2 in Supporting Information S1). For a fairer comparison, the final results are shown for the period 2010–2015, as it is the common period in which the assimilation of the four variables occurs at the same time in the MoLEnKF scheme.

Correctly relating spatial patterns to models also mitigates the fact that hydrological variables are not directly observed by most remote sensors, but are inferred from models linking the observed variable to some hydrologically relevant variables, which introduces an additional source of uncertainty (Nijzink et al., 2018). Consequently, during the assimilation process we moved from using absolute values obtained by remote sensing products to the use of relative values (e.g., anomaly and standard anomaly) for the following observations.

Water level series from ***radar altimetry*** (hereinafter referred to as WSE) were assimilated in each unit-catchment corresponding to the river reach where the VS is located. Because the altimetric reference system is different between the satellite missions and the one used in the MGB model, the assimilation is performed using the water level anomaly. The anomalies values are calculated from the long-term simulation (2002–2020) by discarding the warm up period. The localization is set along the river drainage network starting with a correlation of one (1) in the same unit-catchment where the VS is located and decreasing to zero (0) in distant regions, determined by the distance along the drainage network following a fifth-order function (Gaspari & Cohn, 1999; Hamill et al., 2001; Houtekamer & Mitchell, 2001; Wongchuig et al., 2019). The uncertainty value assumed for all virtual stations was 30 cm, which comes from the accuracy estimate for ENVISAT (Silva et al., 2010).

The assimilation of the ***terrestrial water storage*** component (hereinafter referred to as TWS) assumed the aggregation of pixels within each of the eight large sub-basins (see Figures 1 and 4ii). This is because previous works have shown that GRACE may only be capable of detecting monthly changes in terrestrial water storage over regions larger than 200,000 km² or seasonal changes over areas greater than 184,000 km² (Rodell & Famiglietti, 2001, 2002). Likewise, the assimilation of this variable is in terms of anomalies due to the nature of the information provided by GRACE. The location scheme has been limited to each large sub-basin in terms of its average stored water (see Figure 4ii). According to Zaitchik et al. (2008), to realize the full potential of GRACE for hydrology, the derived regional-scale monthly TWS anomalies must be disaggregated in time. Thus, an approach of downscaling to a temporal resolution of 5 days was performed as evaluated by Shokri et al. (2018) and N. Tangdamrongsub et al. (2015). In which mainly the latter establishes this time interval (5 days) as optimal by trial-and-error to avoid a potential abrupt change as discontinuities as mass (TWS) is added or removed from the state by assimilating temporally very discontinuous values (e.g., monthly) and thus avoiding instability in the DA scheme. For interpolation, we used a simple cubic spline scheme in this study. The total errors found for the ARB by Landerer and Swenson (2012) were assumed as the level of uncertainty, which are around 11.3 mm, slightly lower than the conservative values of 20 mm considered by Wahr et al. (2006) and Zaitchik et al. (2008).

The ***flood extent*** (hereinafter referred to as FE) series were assimilated into MGB considering the accumulated area in large sub-basins (see Figure 1b). It allows the physical continuity of the flooded areas considering that the resolution of the GIEMS-2 pixel (~773 km²) is larger than the average area of the unit-catchments (~320 km²). To avoid numerical errors in the assimilation of variables with a very low temporal resolution (monthly) as in the case of GIEMS-2, and considering that the temporal series of flood extent at large scale are smoothed by the aggregation of several unit-catchments values, a downscaling from monthly values to a temporal resolution of 7 days using a cubic spline was performed. As shown by Ayan Santos Fleischmann et al. (2022) using 29 inundation databases in the ARB, there is a high divergence among the various estimates regarding bias and amplitude. Therefore, in this study we assumed the normalized anomaly of the flood extent to be assimilated and
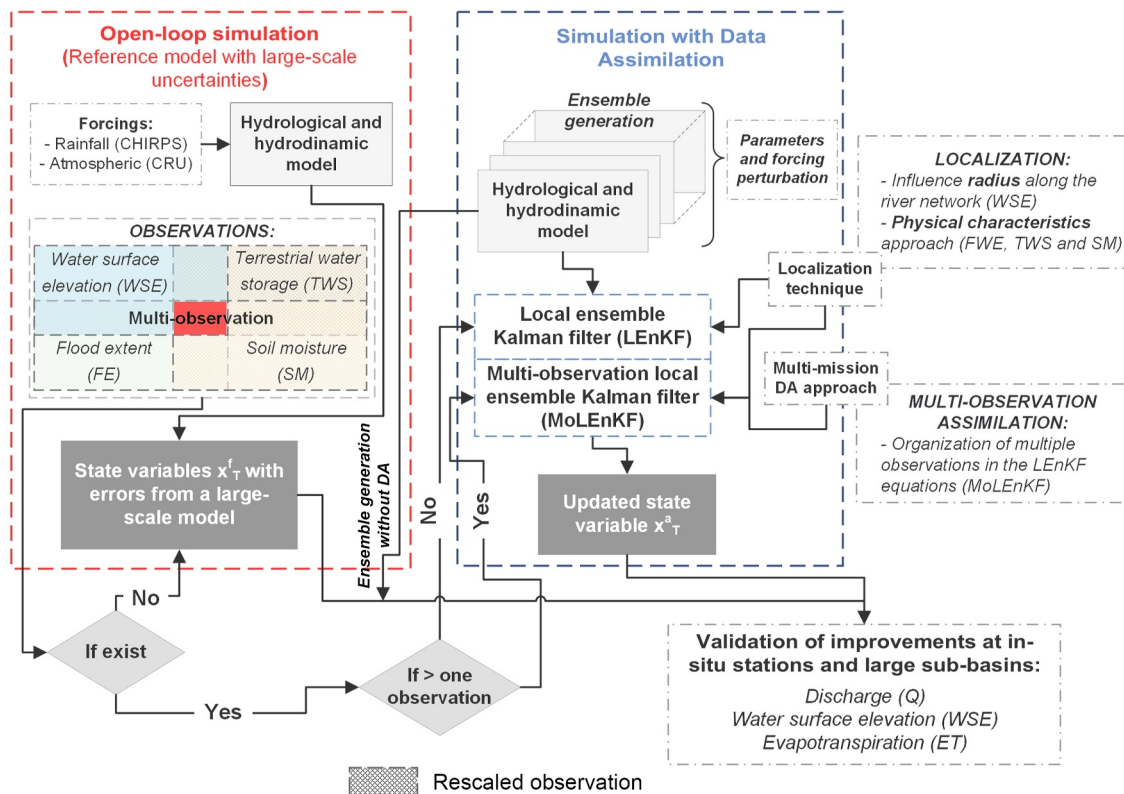
Figure 5. Experimental design, which represents the stages of the simulation within the dotted rectangles for open-loop (red) and assimilation (black).

was calculated from the long-term simulation (2000–2020). In MGB a new state variable had also to be added, which is equivalent to the accumulated area extension of unit-catchments within each of the eight large sub-basins (see Figures 1 and 4ii). Likewise, the localization scheme assumes that there is only correlation ($\rho = 1$) at each large sub-basin independently, as evaluated in the case of the assimilation of TWS.

In MGB, *soil moisture* as a saturation degree was computed as the water in the soil compartment divided by the maximum water capacity of the soil (*Wm* parameter). Since MGB estimates saturation degree for a soil bucket reservoir, RZSM values from SMOS were rescaled for the range 0%–100% according to the min-max correction method described by Albergel et al. (2010) and A. Tarpanelli et al. (2013), and applied in recent studies (e.g., Oliveira et al., 2021; Rajib et al., 2016; Silvestro et al., 2015). In addition, only pixels with a quality value (ancillary data) greater than 0.8 were considered. Thus, rescaled soil moisture (hereinafter referred to as SM) is ingested by DA into MGB on a daily time scale as the weighted average of the unit-catchments within each of the 63 sub-basins, which are referred as calibrated sub-basins (see Figure 4iii) because they add the same set of caliberable parameters in MGB as the *Wm* parameter, then the weighting is done considering the representativeness of the area of this parameter in each of the unit-catchments and hydrologic response units.

Figure 5 shows the general scheme of the experiment setup as (a) the open-loop which is considered here as the mean of the ensemble of the perturbation forcing and model parameters with a certain level of uncertainty, (b) the DA when having one or more observations, and (b) the validation process with in-situ observations.

Table 2 shows the list of state variables of the MGB model that were indicated to be updated in this study.

The performance of the simulations was evaluated by the relative root mean square error (ΔRMSE), calculated for each updated state variable that is, water level, discharge and evapotranspiration. The root mean square error is calculated as follows:

$$\text{RMSE} = \sqrt{\frac{\sum\limits_{i=1}^{N}(S_i - T_i)^2}{N}} \tag{20}$$

$$\Delta\text{RMSE} = \frac{\text{RMSE}_{\text{assimilation}} - \text{RMSE}_{\text{open-loop}}}{\text{RMSE}_{\text{open-loop}}} \tag{21}$$

where N is the number of days of the windows simulations, S represents the simulation (i.e., open-loop, DA LEnKF), T represents the true model. The ΔRMSE compares the performance (decreasing of errors) of the model simulation using the DA scheme with respect to the open-loop (free run simulation).

To measure the uncertainty of the model and the changes when using the proposed methodology, a simple indicator of dispersion of the ensemble realizations was used, in this case the standard deviation and its percentage variation, where negative values indicate a decrease in dispersion.

For the daily time series of discharge and water level the Nash–Sutcliffe efficiency (NSE), the Kling–Gupta (KGE) and the absolute value of volume error (hereafter referred to as BIAS) were also assessed The NSE is a normalized statistic that determines the relative magnitude of residual variance compared with the observed data variance, while the KGE offers interesting results in model performance, because it uses the most components, such as correlation, variability and bias terms. Both NSE and KGE range between $-\infty$ and 1 (perfect fit).

$$\text{NSE} = 1 - \frac{\sum\limits_{i=1}^{nt}(Q_{\text{obs}}(t) - Q_{\text{sim}}(t))^2}{\sum\limits_{i=1}^{nt}(Q_{\text{obs}}(t) - \overline{Q_{\text{obs}}})^2} \tag{22}$$

$$\text{KGE} = 1 - \sqrt{(r-1)^2 + \left(\frac{\sigma_{\text{sim}}/\mu_{\text{sim}}}{\sigma_{\text{obs}}/\mu_{\text{obs}}} - 1\right)^2 + \left(\frac{\mu_{\text{sim}}}{\mu_{\text{obs}}} - 1\right)^2} \tag{23}$$

$$\text{BIAS} = \left| \frac{\sum\limits_{i=1}^{nt}(Q_{\text{sim}}(t)) - \sum\limits_{i=1}^{nt}(Q_{\text{obs}}(t))}{\sum\limits_{i=1}^{nt}(Q_{\text{obs}}(t))} \right| \tag{24}$$

Six experiments were performed: the first one corresponds to the simulation without assimilation (hereafter called "open-loop"), the next four others are the assimilation of individual data sets, and the final corresponds to the assimilation of multiple observations.

3. Results and Discussions

This section is divided in two parts, the first one discusses the relative improvements of the five DA experiments compared to the open-loop simulation, which assumes in this study the uncertainties of a large-scale model (e.g., continental, global). In this way we document the reduction of errors and uncertainties of each experiment in this context, and quantify the potential benefits of the MoLEnKF technique compared to univariate assimilation. The second part discusses the overall performance of the single and multi-observation (MoLEnKF) DA experiments, focusing more on the latter, as well as discussing the results of similar models implemented/documented for the ARB in recent studies.

3.1. Impact of the DA From Remotely Sensed Observations on Simulations of a Large-Scale Uncertain Model

In this subsection, we discuss the results of each DA experiment and the reduction of errors and uncertainty of the daily discharge, water level and monthly actual evapotranspiration estimates in comparison to the open-loop simulation.

Figure 6a shows the seasonal climatological variability of discharge estimation at five in-situ gauging stations, relative to the assimilation of individual remote sensing products and with the MoLEnKF approach by assimilating the four observations at the same time. These stations were chosen because they are representative of the contribution regions of different important parts of the ARB. For example, Tamshiyacu station receives the contribution of discharge from the western region of the ARB, whose main tributaries are the Ucayali and Marañon rivers from Peru. Likewise, the Porto Velho station agglomerates the discharge of the southern region of the ARB belonging to the Madeira River which originates in the country of Bolivia. The Itautaba station agglomerates the Tapajós River of the southeastern region of the ARB, the São Felipe station of the Negro River to the north of the ARB and the Óbidos station which has the largest contributing area in the ARB. It should be noted that the performance was analyzed with a daily time series. Overall, the aggregation of the monthly climatology of the observed and simulated discharge time series and the boxplot (inserted in each panel) indicate that the largest error reductions (ΔRMSE) were achieved mostly by the WSE (light blue line/circle) and the MoLEnKF (red line/circle) DA experiments. This error reduction for all stations reaches a median value of ∼36% and ∼33% for WSE and MoLEnKF, respectively (see Figure 6d). The latter is shown as an average performance of the four univariate experiments. A similar performance occurs when analyzing the reduction of the dispersion (Figure 6b) of the analyzed realizations by their standard deviation. Although the absolute values depend on the average discharge at each station, this relative reduction in percentage terms reaches values of ∼23% and ∼16% through the assimilation of WSE and MoLEnKF, respectively (see Figure 6e). While the error reduction is relatively high in many of the cases (Figure 6c), the largest error reductions are estimated in the upper Negro, Tapajós, upper Madeira and lower Amazon River sub-basins considering the WSE, TWS, FE and MoLEnKF DA experiments. The lowest error reduction was obtained by assimilating SM, which are mainly observed in the Tapajós river. This spatial analysis may be important in the context of future experiments where it is necessary to localize the required performance by assimilating specific remote sensing missions within a large-scale model such as MGB. When analyzing stations with a larger contributing area (>25,000 km^2) (not shown), the ΔRMSE values in the WSE and MoLEnKF experiments reach values of ∼−40% and ∼−38%, respectively.

In the case of validation of the daily water level series at five in-situ gauging stations, this section shows the results at the Tabatinga station instead of Tamshiyacu which has not documented water level data (see Table S1 and Figure S1 in Supporting Information S1). It is observed from the boxplots (Figure 7a) that similar to the daily discharge validation, in these five stations error reduction is consistently present in the WSE and MoLEnKF experiments. Reaching values of −38% and −34% respectively for median values in the 87 stations analyzed (see Figure 7d). In addition, it led to ΔRMSE values of −47% and −42% in the WSE and MoLEnKF experiment, respectively for stations with larger contributing areas (>25,000 km^2) (not shown). It is interesting to note that the greatest reduction of errors when assessing water level occurs when assimilating the same variable, which is coherent and already observed for example, by Wongchuig, Cauduro Dias de Paiva, et al. (2020) when assimilating pseudo-observations from the SWOT mission. In that study, ΔRMSE also reached high values (−36%) when assimilating and validating WSE anomalies, which is mainly explained by two aspects. First, that a reference model (open-loop) was similarly configured so that it represents global model uncertainties by altering more forcings and model parameters. In other words, in situations of greater uncertainty, the scheme presented in this study could achieve greater error reduction. Second, the fact that the error reduction is slightly lower than in the present study is possibly because of the validation was not performed at the level of in-situ observed stations but at the unit-catchment level, that is, with areas of contribution with a median of ∼3,400 km^2. In terms of error reduction, Figure 7b shows that these are relatively higher than in the discharge analysis, reaching average values from 6 m for the open-loop to values of 1 m or lower in their standard deviation when using DA. This represents a relative reduction of over 80% for all assimilation cases (see Figure 7e). This indicates that the water level estimation is sensitive to the uncertainty of the parameters and forcing's and can be greatly improved in any of the five proposed experiments. The TWS DA experiment also achieves adequate levels of error reduction (larger than the median), as shown at the Porto Velho station (in the Madeira River) and in general in the Tapajós sub-basins and in the upper and lower Madeira (Figure 7b). Meanwhile, also at the spatial level and similar to what was

Figure 6. (a) Daily discharge climatology for in-situ observations (blue line), open-loop (dotted black line) and assimilation runs at five stations. The ΔRMSE performance boxplots for each DA experiment are superimposed. (b) Boxplot of the dispersion for each experiment in the five stations. (c) Map of the DA performance based on the ΔRMSE index. The size of the circles indicates the area of contribution of each station. Boxplot of (d) ΔRMSE and (e) ΔStandard deviation performance for all single and multi-observation (MoLEnKF) DA experiments.

observed in the discharge validation, the smallest error reduction was observed when assimilating SM from SMOS. This can be explained may be due to (a) difficulties in recovering surface soil moisture and root zone moisture in areas of very dense vegetation and (b) the weak connection between soil moisture and discharge in the Amazon basin due to the low slope and high volumes of subsurface water. To some extent this was also concluded by Chen et al. (2011) who showed that SM assimilation, even with root-zone soil moisture products, has a minimal effect on the deep-layer soil simulation, and therefore on the impact of runoff simulations. It is important
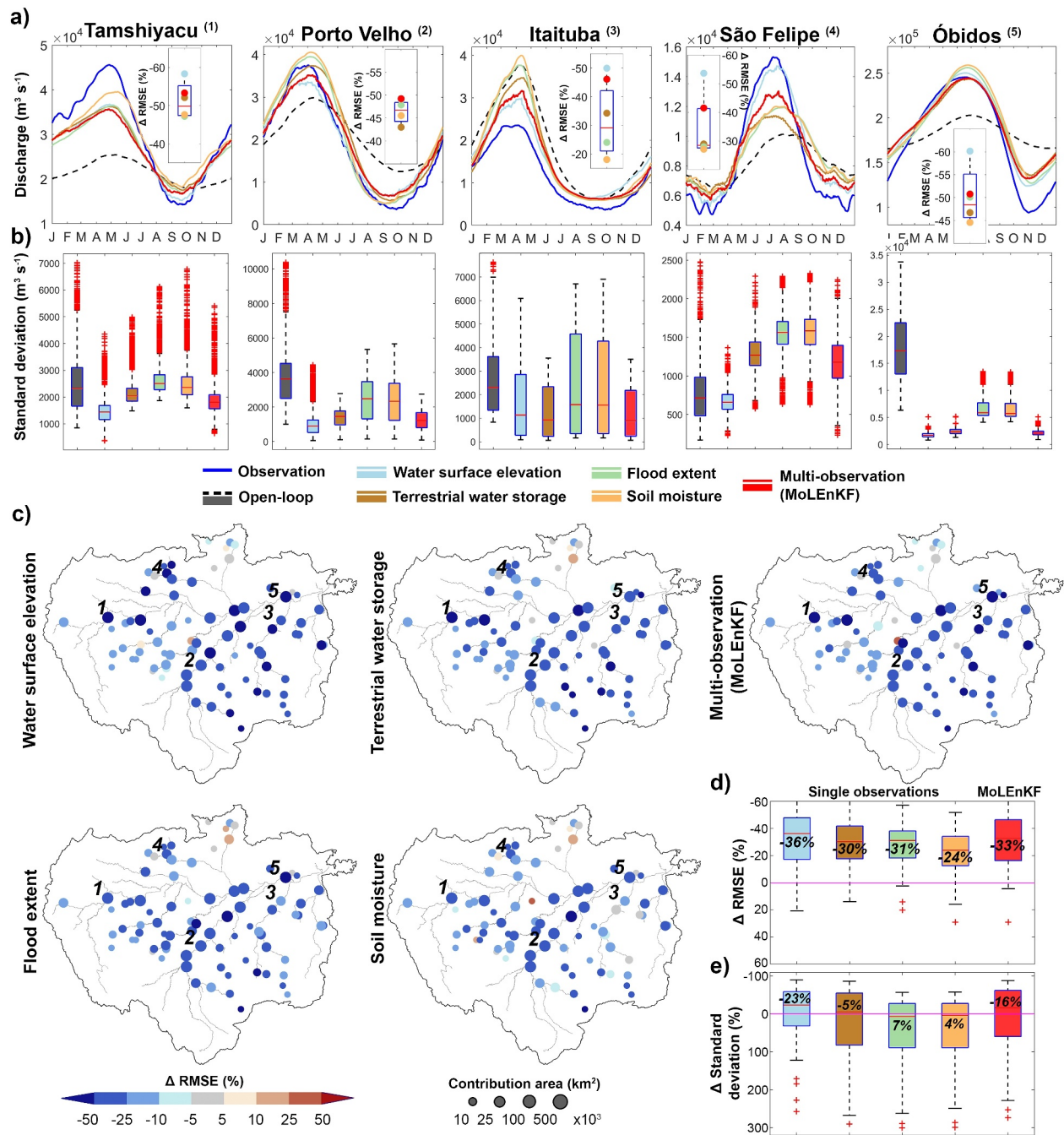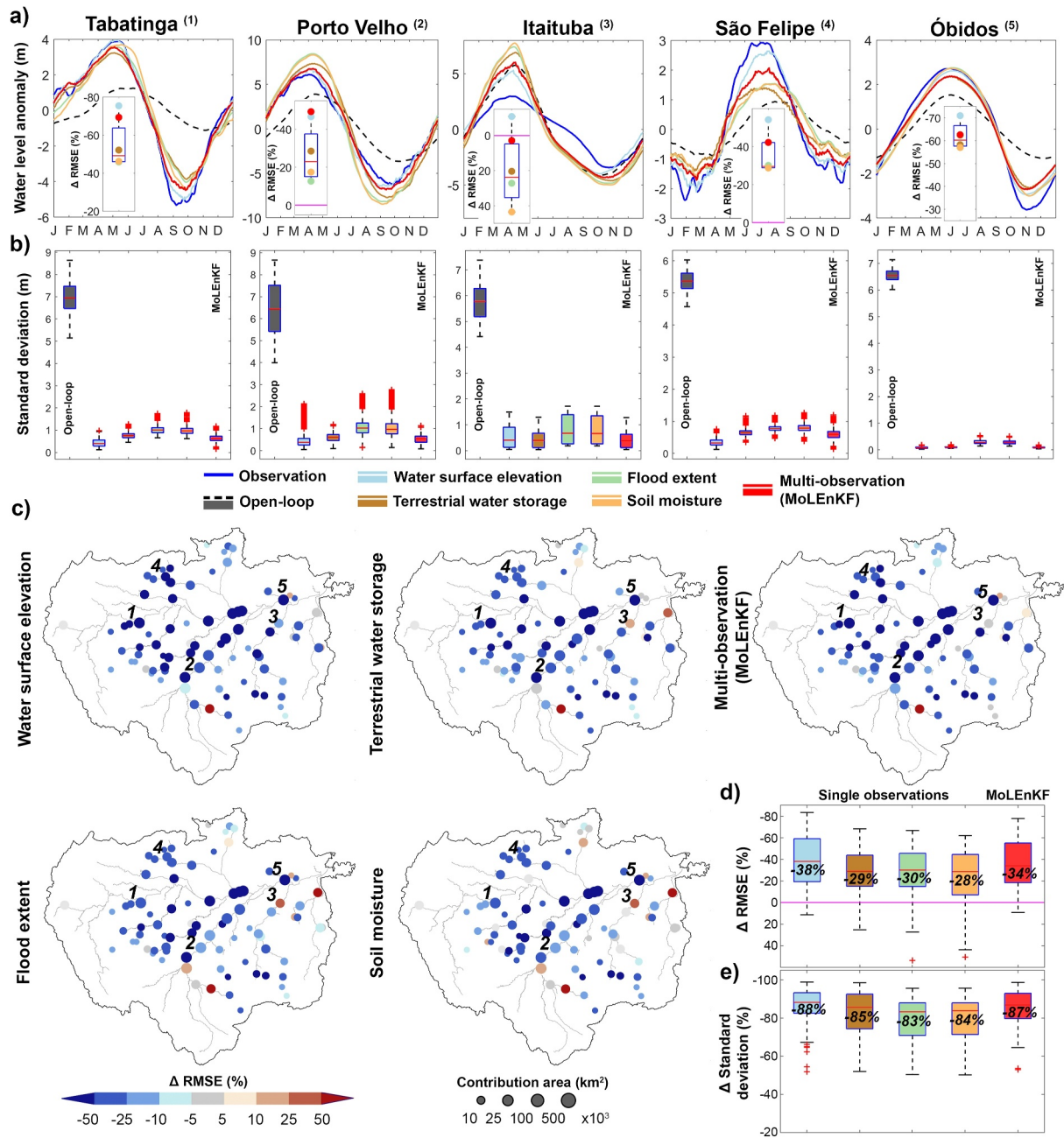
Figure 7. (a) Daily water level climatology for in-situ observations (blue line), open-loop (dotted black line) and assimilation runs at five stations. The ΔRMSE performance boxplots for each DA experiment are superimposed. (b) Boxplot of the dispersion for each experiment in the five stations. (c) Map of the DA performance based on the ΔRMSE index. The size of the circles indicates the area of contribution of each station. Boxplot of (d) ΔRMSE and (e) ΔStandard deviation performance for all single and multi-observation (MoLEnKF) DA experiments.

to note that error reduction by assimilating WSE and multiple observations (MoLEnKF) occurs in more than the 90% of all validated in-situ stations. Spatially, considering the general performance of all in-situ gauges, largest improvements were achieved in the western and in the central ARB located in the sub-basin of the Amazon upstream and Madeira River, respectively.

Figure 8 shows the seasonal climatological variability of estimated and ET-Amazon evapotranspiration in eight large sub-basins. Performance analyses were assessed at the monthly level. It can be seen from the time series (Figure 8a) that the performance among open-loop and DA experiments varies according location. In the northern
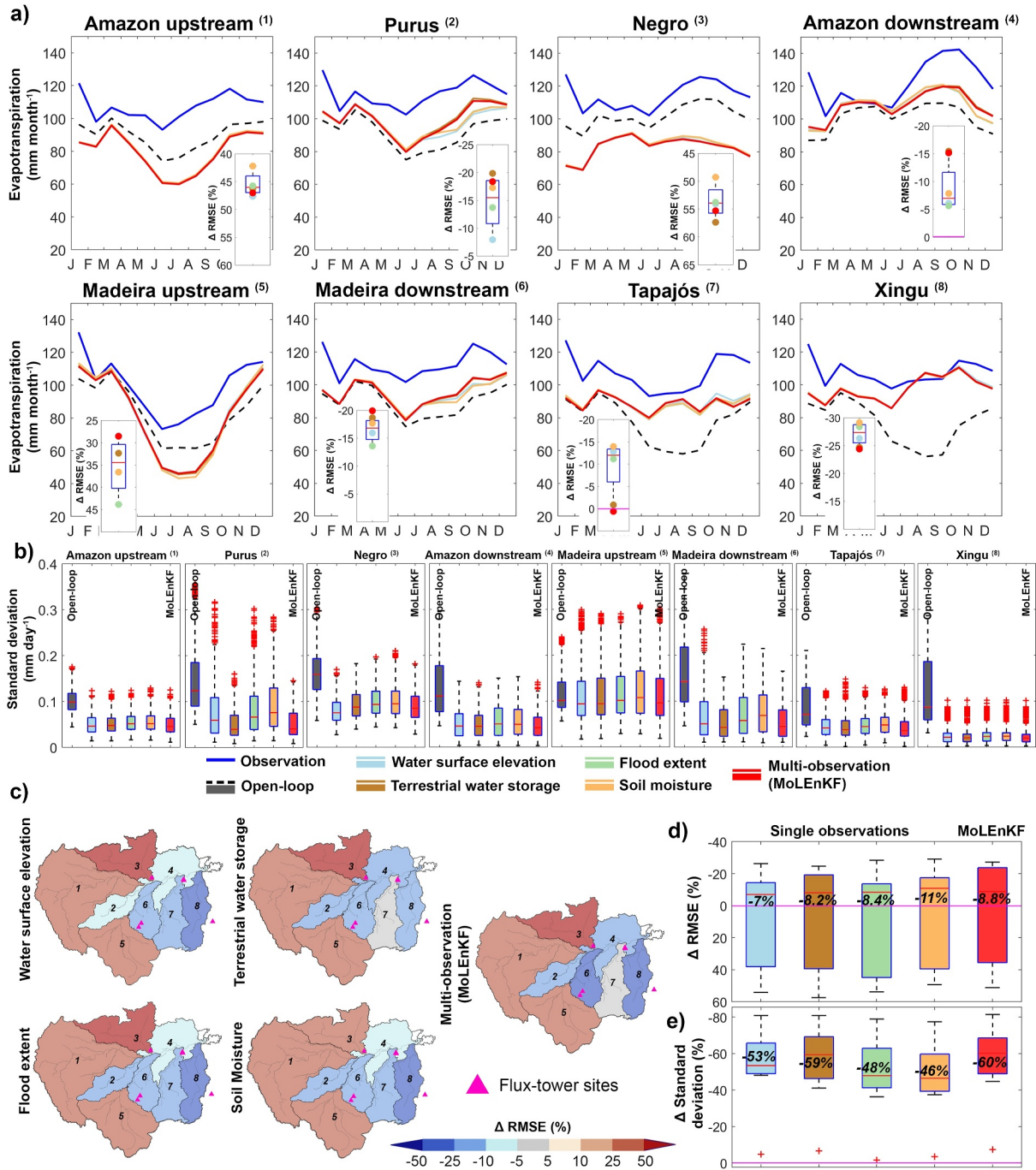
Figure 8. (a) Climatology of monthly evapotranspiration time series for observations (black), open-loop (dotted black) and assimilation simulations, for eight large sub-basins. (b) Boxplot of the dispersion for each experiment in the eight large sub-basins. (c) Map of the performance of the simulations with assimilation from the ΔRMSE index. Boxplot of (d) ΔRMSE and (e) ΔStandard deviation performance for all single and multi-observation (MoLEnKF) DA experiments.

Amazon region such as the Negro River sub-basin, the simulations hardly capture the seasonality, mainly during the period from July to December, which may probably due to two reasons, (a) a large divergence in the representation of FWE and thus in the estimation of open water evaporation between MGB estimates and the ET-Amazon product, and/or (b) the lack of an adequate representation of climate forcing in the MGB used to estimate evapotranspiration. In fact, errors increase with a tendency toward underestimation, which also occurs in the western and southern regions in the upper Amazon and Madeira sub-basins (Figure 8c). It is interesting to see that error reduction is mainly localized in regions close to the flux towers used to produce/validate the ET-Amazon

Figure 9. Summary of the median values of the improvement in the (a) errors and (b) uncertainty in each state variable (discharge, water level and evapotranspiration) for each single and multiple observation assimilation experiment (MoLEnKF).

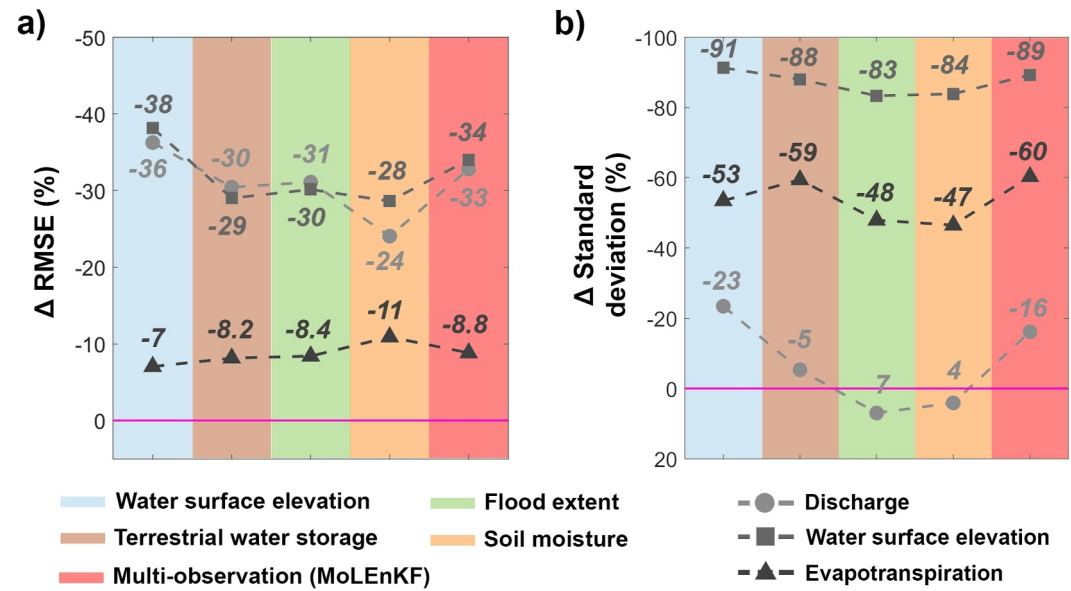database. This may indicate a scenario where improvements in the DA technique are primarily observed in regions where the reference database is more reliable, whereas in other regions there may have indeed been an improvement in ET simulations by MGB. It can also be noted that in these specific regions, the simulations aggregate better with observations at the seasonality level, such as in the Tapajós and Xingu sub-basins.

In general, Figure 8d shows that the error reduction has not been as high as in discharge or water level; however, they reach values of −11% for the experiment assimilating SM, which would indicate that within the MGB, this variable largely controls the evapotranspiration processes in the ARB. Similarly, the reduction in dispersion shown in Figures 8b and 8e indicates that the MoLEnKF assimilation achieves higher reduction values, with median values across the eight major sub-basins of −60%.

To sum up all of these results, Figure 9 shows the median values of error and uncertainty reduction in the estimation of discharge, water level, and evapotranspiration when each DA experiment is performed. It is observed that the greatest improvement in the errors of the hydraulic variables (discharge and water level) occurs when assimilating WSE, while the univariate assimilation of TWS, FE, and SM maintains a similar performance of around −30% in error reduction for both discharge and water level, while the MoLEnKF experiment shows an average performance of the four previous ones (∼−33%).

It is important to highlight here that the added benefit of implementing multivariable assimilation is observed when evaluating, in addition to hydraulic variables, others such as evapotranspiration, where assimilating SM shows greater error reduction than assimilating WSE. This ultimately impacts the performance in the MoLEnKF experiment, reinforcing the message of other studies (e.g., Girotto et al., 2019; Khaki et al., 2020; S. V. Kumar et al., 2019) indicating that the simultaneous assimilation of multiple observation data strongly improves model predictions compared with single observation and/or state estimation alone. In general, the smaller reduction in errors observed when validating evapotranspiration compared to discharge and water level can be explained mainly by two things, (a) that the evapotranspiration in Amazon depends much on available energy, and in the DA strategy there is no perturbation on climate forcing other than precipitation (i.e., radiation) and (b) the evapotranspiration by itself is not considered as a state variable but rather a water/energy flux, therefore not directly updated in the DA scheme. Furthermore, the impact on uncertainty reduction (Figure 9b) follows a similar pattern to error reduction, where typically the WSE DA experiment shows greater reductions (except in evapotranspiration), while the MoLEnKF exhibits an average reduction, surpassing all in reducing evapotranspiration uncertainty.

In a comparative manner, and to verify the impact on overall error and uncertainty reduction of each experiment, the Supporting Information S1 shows (Figure S4) the results of a complementary experiment in which the background model (open-loop) only considers precipitation uncertainties for generating ensemble members, in a model configuration where hydraulic and hydrological parameters are calibrated based on the version of Siqueira et al. (2018) and Wongchuig et al. (2019). In this scenario, it is also observed that, although the error reduction is lower because the reference model only represents precipitation uncertainties, the WSE DA experiment shows better performance in discharge and water level but not in evapotranspiration, consistently leaving the MoLEnKF experiment in a second position in an error reduction ranking across all scenarios. This robustly demonstrates that the MoLEnKF experiment has the advantage of being able to reduce errors more holistically than a single variable.

Furthermore, highlighting the potential of these results, such as in operational forecasting systems, which focus primarily on river discharge and water level DA techniques, rather than evapotranspiration. In this study we focus on quantifying improvements in other components of the hydrologic cycle, not only for possible improvements in forecasting systems but also for the development of hydrological reanalysis. For example, involving ingesting as much observed data as possible with the goal of making predictions of hydrologic cycle variables rather than local improvements in river discharge or water level.

3.2. Overall Performance of the Single and Multi-Observation (MoLEnKF) DA Experiments

In this subsection we show the results of the overall performance of the DA experiments according to their bias, amplitude and volume mainly represented in the KGE, NSE and BIAS indices. We mainly focused on the MoLEnKF experiment by also comparing it with the validated outputs of referenced hydrologic-hydrodynamic models documented in other studies such as the MGB and CaMa Flood in the ARB. These versions are denoted as (1), (2), (3) and (4), for the models applied in the ARB. (1) is the calibrated version of the MGB model for South America, by Siqueira et al. (2018), (2) version of the MGB model with assimilation of daily discharge data and referred to as the twentieth Century Hydrological Reanalysis of the Amazon, by (Wongchuig et al., 2019), (3) version of the CaMa Flood model with radar altimetry assimilation, by Revel et al. (2023) and (4) version of MGB model where satellite altimetry from virtual stations and in-situ discharge data were assimilated, by (Rodrigo C.D. Paiva et al., 2013).

The performance for 85 in-situ river gauge stations is presented in Figure 10. The lowest BIAS was achieved by MoLEnKF of the four variables, reaching ~19.8%. Despite the overall reduction of BIAS in all experiments in respect to the open-loop (~30% of reduction), these are still relatively high compared to the other MGB model versions (1) and (2). The lower BIAS values achieved by (2) may be due to the rainfall forcing undergoing a bias correction process. The highest performance, in this study, in the KGE and NSE indices was achieved by WSE assimilation with median values of 0.7 and 0.64, respectively. Compared to studies (1), (2), (3) and (4), the best performances were achieved by (2) using the MGB model, with a KGE index of 0.75, which is based on assimilation of daily discharge data. Among these, the study (4) stands out with the highest NSE value of 0.68, which can be explained because, in addition to assimilating radar altimetry, in-situ discharge was also assimilated. However, the results of the present study from the MoLEnKF experiment show a better performance than that of (3), where the normalized anomaly of WSE from virtual stations was assimilated, with mean values of NSE and KGE of 0.47 and 0.62, respectively. At a spatial level, the present study and the four compared ones agree that the best performance occurs in the central region of the ARB, such as in the Purus rivers, the lower part of the Negro and Madeira rivers, where river discharge was reliably estimated.

Figure 11 shows the performance of water level at 87 in-situ gauging stations. The best performance is achieved by assimilating WSE and MoLEnKF, which reduces bias, errors and improves the NSE index. Regarding BIAS, the assimilation of TWS and FE also achieved relative adequate values, which were initially small in the open-loop. In contrast, the SM DA experiment increased the BIAS to 2.5%, doubling the initial overestimation of the open-loop. This particular experiment also resulted in lower NSE and RMSE performance, reaching values of 0.78 and 1.53 m, respectively. This poor performance in discharge and water level estimation when assimilating SM can be possible explained by the fact that the runoff generation in the MGB model is based on the saturation-excess scheme (runoff is generated when the soil is fully saturated). Therefore, when the soil compartments are directly updated by the DA technique, it may not necessarily alter the runoff if the soil is not yet saturated. As a result, the impact on discharge and water level is not as significant, even though these latter state variables are also
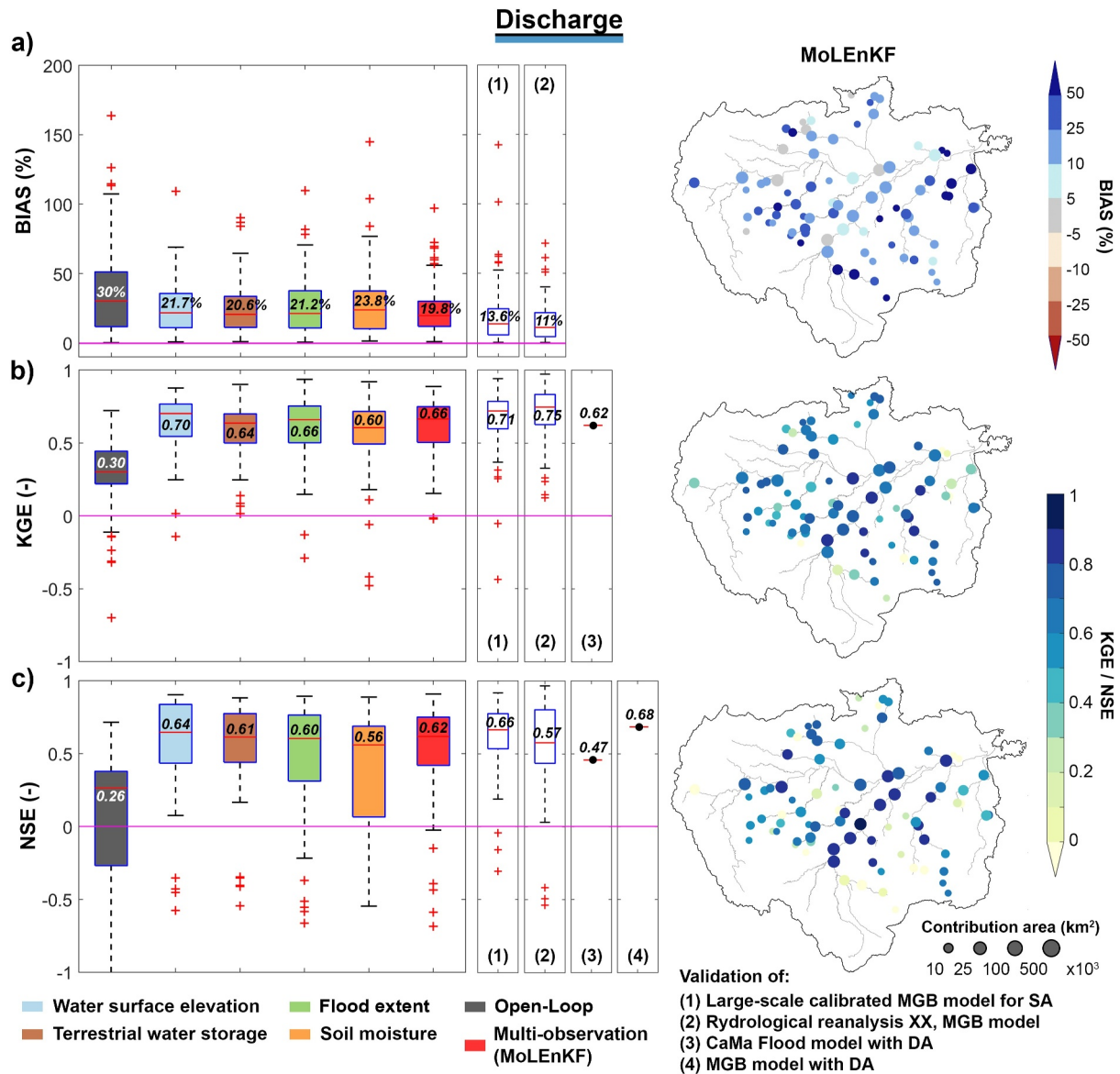
Figure 10. (a) Boxplot of performance for discharge on BIAS, KGE and NSE for open-loop and assimilation of single and multi-observation (MoLEnKF) experiments. Boxplots for each statistical index of studies (1), (2), (3) and (4) are positioned on the right. (b) Maps of performance for discharge on BIAS, KGE and NSE for the MoLEnKF assimilation experiment at 85 in-situ gauging stations. The size of the circles indicates the area of contribution of each station.

updated in the DA scheme. At least ∼60% of the gauging stations achieved a NSE higher than 0.75 at daily time steps for both WSE and MoLEnKF experiments, with median values of 0.88 and 0.84, respectively. These results are comparable with other studies such as the one by Paiva et al. (2013) (4) where radar altimetry assimilation was performed in the ARB, reaching average levels of 0.74 of NSE. Considering the univariate DA experiments, the DA of TWS performs better than SM and FE, which can be explained because of (a) low level of aggregation after the rescaling process of the SM variable, and the lack of physical representation of the process within MGB, which considers one only soil bucket; (b) the high uncertainty of the FWE products, and (c) the uncertainty in the hydraulic parameters of MGB representing the floodplain topography and channel bankfull properties. Figure 11c shows that the largest errors when performing the MoLEnKF assimilation are located mainly in the upper part of the Purus sub-basin. Overall, the median of these errors, reaching 1.02 m, remains below those found in a calibrated model (a), and even more accurate than a study (3) where the altimetry anomaly is also assimilated. In general, the MoLEnKF assimilation performance reaches levels close to the WSE experiment, and these adequate
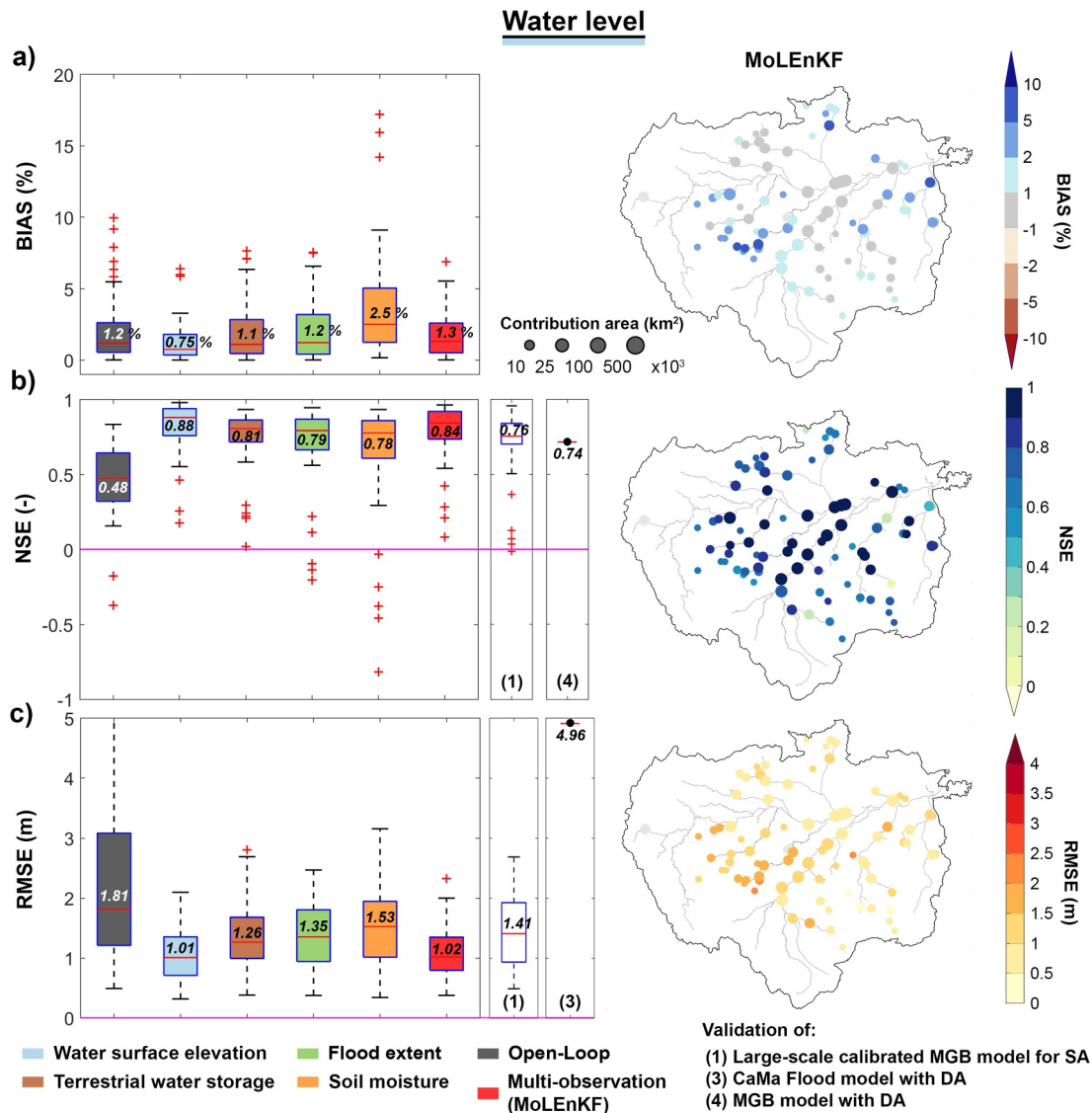
Figure 11. (a) Boxplot of performance for water level on BIAS, NSE and RMSE for open-loop and assimilation of single and multi-observation (MoLEnKF) experiments. Boxplots for each statistical index of studies (1), (3) and (4) are positioned on the right. (b) Maps of performance for water level on BIAS, NSE and RMSE for the MoLEnKF assimilation experiment at 87 in-situ gauging stations. The size of the circles indicates the area of contribution of each station.

level performances are evenly distributed throughout the basin. Therefore, once the results in this section have been demonstrated, it is evident that the MoLEnKF scheme solely assimilating remote sensing information is capable of achieving levels of efficiency, and in many cases surpassing results from studies where in-situ information and/or prior calibration processes are utilized.

4. Conclusion and Perspectives

In this study we provide an assimilation framework that is designed for multiple and multiscale data assimilation, a major contribution when compared to many previous studies that intercompare the results of assimilation schemes of one or two products only. The proof of concept presented in this study is based on the local ensemble Kalman filter (LEnKF) technique implemented on a large-scale hydrologic-hydrodynamic model. This methodological approach is referred to in this study as MoLEnKF. We evaluated the performance of four independent observation assimilation experiments together with an experiment assimilating all four observations at the same time, when available, using the Amazon River Basin (ARB) as a case study. It is interesting to highlight that our background model is a version representing uncertainties of large-scale hydrological-hydrodynamic models, such

as continental or global ones. Thus, in this study, we have been able to quantify the improvements achieved with the MoLEnKF technique when only remote sensing observations/data sets have been used in the assimilation process. This is highly important in the context of replicability in other regions with scarce or no in-situ hydroclimatic records, which are typically used for model calibration, and where only globally available remote sensing databases could be utilized.

The improvements of an uncertain large-scale hydrological-hydrodynamic model shows that in overall, assimilating water surface elevation anomaly (WSE) from radar altimetry led to the best performance for discharge and water level estimation from all individual experiments, reducing RMSE in discharge and water level simulation by 36% and 38%, respectively. However, the greatest reduction in evapotranspiration RMSE was achieved through SM DA, with median values of 11%. Here it is important to highlight that the performance achieved by the MoLEnKF DA experiment, may always achieve values consistently ranked second, sometimes below water surface elevation anomaly (WSE) DA and other times below soil moisture (SM) DA when different variables are validated (e.g., discharge, water level, and evapotranspiration) as shown above. MoLEnKF achieved reductions in errors (RMSE) of 33%, 34%, and 8.8% for discharge, water level, and evapotranspiration, respectively, evaluated in drainage areas exceeding 10,000 km^2 and large sub-basins.

These results also bring us back to the debate of which factor is more important in DA schemes using the Kalman filter technique: the temporal frequency or the spatial resolution of the observations? This provides an interesting perspective to be analyzed using the MoLEnKF DA scheme proposed here, considering that, in many cases, a drawback of DA remote sensing data sets lies in their coarse temporal resolutions. For example, to effectively monitor flash flood dynamics, the traditionally used DA processes should be performed on daily to hourly time scales; however, the revisit frequency of the satellites used to capture WSE is on the scale of tens of days. In this study, many of these uncertainties were implicitly quantified by analyzing the dispersion of ensemble realizations before and after the DA process. It is important to emphasize that here it was also observed that the MoLEnKF method also achieves reduction values in dispersion consistently ranked second among all experiments, reaching relative reduction values of 16%, 89%, and 60% for discharge, water level, and evapotranspiration, respectively. These and previous results demonstrate that the MoLEnKF experiment has the advantage of being able to reduce errors and uncertainties in a more holistic manner than univariate DA experiments.

Here the MoLEnKF DA scheme can improve the simulations of an uncertain large-scale hydrologic-hydrodynamic model and establish similar and, in some cases, even better values than state-of-the-art models at these temporal and spatial scales considering discharge and daily water level with NSE metrics of 0.62 and 0.84, respectively. This is even more remarkable in the context that only remote sensing data were used in the assimilation process. This also may bring prospects for future studies for the correction/updating of model parameters in a sequential calibration scheme, where the effectiveness of EnKF in spatially distributed hydrologic-hydrodynamic models has not yet been extensively tested.

It is important to highlight the simple and elegant way of expressing the matrix arrangements in the equations of the LEnKF technique adopted in this study. Even though, there are important perspectives for further improvements, assuming for example, a certain degree of correlation between the different assimilated variables in the multi-observation assimilation scheme. The same applies for the localization method, in which the radius of influence is fixed in time, and which can be more explored by a temporal variation according to the seasonal periods. Likewise, the localization techniques presented in this study for TWS and SM assimilation from GRACE and SMOS, respectively, are a first spatial approximation that requires further exploration, as well as to evaluate additional spatial rescaling methods to those proposed here. Additionally, it is fundamental to further improve the physical consistency between model outputs and observations of some variables that are not directly observed by remote sensing, such as soil moisture or evapotranspiration.

Thanks to its flexibility and robustness, the MoLEnKF DA methodology can be applied with several sets of variable types compatible with those state variables of large-scale hydrological-hydrodynamic models, including those available in the SWOT mission launched in December 2022. This mission will provide a great opportunity due to its advantages in terms of spatio-temporal resolution and accuracy compared to current missions. Finally, its easy replicability in other regions around the world, as mentioned at the beginning of this section, may also allow to generate a coherent record (hydrological reanalysis) covering the last decades of the satellite era. In addition, it can establish the technical basis for more accurate hydrological-hydrodynamic forecasting due to the improved updating of the initial conditions of the model state variables.

Data Availability Statement

All the data used in this study are open source, and publicly available (access date October 2023): MGB model main branch version (https://github.com/HGE-IPH/MGB). CHIRPSv2 (https://data.chc.ucsb.edu/products/CHIRPS-2.0/global_monthly/netcdf/). GRACE and GRACE-FO (https://search.earthdata.nasa.gov/search?portal=podaac-cloud). Water level estimations from satellite altimetry (http://hydroweb.theia-land.fr/). SMOS L4RZSM (https://www.catds.fr/Products/Catalogue-CPDC/Catds-products-from-Sextant#/metadata/316e77af-cb72-4312-96a3-3011cc5068d4). River discharge and water level in-situ observations (http://www.snirh.gov.br/hidroweb/). ET-Amazon (https://www.hydroshare.org/resource/24792a48a6394dcba52da62fa324ae40/).

References

Abbaszadeh, P., Gavahi, K., & Moradkhani, H. (2020). Multivariate remotely sensed and in-situ data assimilation for enhancing community WRF-Hydro model forecasting. *Advances in Water Resources*, *145*, 103721. https://doi.org/10.1016/j.advwatres.2020.103721

Aires, F., Prigent, C., Fluet-Chouinard, E., Yamazaki, D., Papa, F., & Lehner, B. (2018). Comparison of visible and multi-satellite global inundation datasets at high-spatial resolution. *Remote Sensing of Environment*, *216*(July 2017), 427–441. https://doi.org/10.1016/j.rse.2018.06.015

Albergel, C., Calvet, J.-C., de Rosnay, P., Balsamo, G., Wagner, W., Hasenauer, S., et al. (2010). Cross-evaluation of modelled and remotely sensed surface soil moisture with in situ data in south western France. *Hydrology and Earth System Sciences*, *14*(11), 2177–2191. https://doi.org/10.5194/hess-14-2177-2010

Al Bitar, A., Kerr, Y., Merlin, O., Cabot, F., & Wigneron, J.-P. (2013a). Global drought index from SMOS soil moisture. In *IEEE international geoscience and remote sensing symposium, IGARSS 2013*. Retrieved from https://hal.inrae.fr/hal-02805746

Al Bitar, A., Kerr, Y., Merlin, O., Cabot, F., & Wigneron, J.-P. (2013b). Global drought index from SMOS soil moisture. In *IEEE international geoscience and remote sensing symposium, IGARSS 2013*.

Al Bitar, A., Mialon, A., Kerr, Y. H., Cabot, F., Richaume, P., Jacquette, E., et al. (2017). The global SMOS Level 3 daily soil moisture and brightness temperature maps. *Earth System Science Data*, *9*(1), 293–315. https://doi.org/10.5194/essd-9-293-2017

Alfieri, L., Avanzi, F., Delogu, F., Gabellani, S., Bruno, G., Campo, L., et al. (2022). High-resolution satellite products improve hydrological modeling in northern Italy. *Hydrology and Earth System Sciences*, *26*(14), 3921–3939. https://doi.org/10.5194/hess-26-3921-2022

Alsdorf, D., Beighley, E., Laraque, A., Lee, H., Tshimanga, R., O'Loughlin, F., et al. (2016). Opportunities for hydrologic research in the Congo Basin. *Reviews of Geophysics*, *54*(2), 378–409. https://doi.org/10.1002/2016RG000517

Andreadis, K. M., Clark, E. A., Lettenmaier, D. P., & Alsdorf, D. E. (2007). Prospects for river discharge and depth estimation through assimilation of swath-altimetry into a raster-based hydrodynamics model. *Geophysical Research Letters*, *34*(10), 1–5. https://doi.org/10.1029/2007GL029721

Andreadis, K. M., Das, N., Stampoulis, D., Ines, A., Fisher, J. B., Granger, S., et al. (2017). The regional hydrologic extremes assessment system: A software framework for hydrologic modeling and data assimilation. *PLoS One*, *12*(5), 1–22. https://doi.org/10.1371/journal.pone.0176506

Andreadis, K. M., Schumann, G. J. P., & Pavelsky, T. (2013). A simple global river bankfull width and depth database. *Water Resources Research*, *49*(10), 7164–7168. https://doi.org/10.1002/wrcr.20440

Anees, M. T., Abdullah, K., Nordin, M. N. M., Rahman, N. N. N. A., Syakir, M. I., & Kadir, M. O. A. (2017). One- and two-dimensional hydrological modelling and their uncertainties. In *Flood risk management* (Vol. i, pp. 1–30). InTech. https://doi.org/10.5772/intechopen.68924

Archfield, S. A., Clark, M., Arheimer, B., Hay, L. E., McMillan, H., Kiang, J. E., et al. (2015). Accelerating advances in continental domain hydrologic modeling. *Water Resources Research*, *51*(12), 10078–10091. https://doi.org/10.1002/2015WR017498

Arnesen, A. S., Silva, T. S. F., Hess, L. L., Novo, E. M. L. M. L. M., Rudorff, C. M., Chapman, B. D., & McDonald, K. C. (2013). Monitoring flood extent in the lower Amazon River floodplain using ALOS/PALSAR ScanSAR images. *Remote Sensing of Environment*, *130*, 51–61. https://doi.org/10.1016/j.rse.2012.10.035

Asadzadeh Jarihani, A., Callow, J. N., Johansen, K., & Gouweleeuw, B. (2013). Evaluation of multiple satellite altimetry data for studying inland water bodies and river floods. *Journal of Hydrology*, *505*, 78–90. https://doi.org/10.1016/j.jhydrol.2013.09.010

Baguis, P., & Roulin, E. (2017). Soil moisture data assimilation in a hydrological model: A case study in Belgium using large-scale satellite data. *Remote Sensing*, *9*(8), 1–26. https://doi.org/10.3390/rs9080820

Barichivich, J., Gloor, E., Peylin, P., Brienen, R. J. W., Schöngart, J., Espinoza, J. C., & Pattnayak, K. C. (2018). Recent intensification of Amazon flooding extremes driven by strengthened Walker circulation. *Science Advances*, *4*(9), eaat8785. https://doi.org/10.1126/sciadv.aat8785

Bates, P. D., Horritt, M. S., & Fewtrell, T. J. (2010). A simple inertial formulation of the shallow water equations for efficient two-dimensional flood inundation modelling. *Journal of Hydrology*, *387*(1–2), 33–45. https://doi.org/10.1016/j.jhydrol.2010.03.027

Bates, P. D., Neal, J. C., Alsdorf, D., & Schumann, G. J. P. (2014). Observing global surface water flood dynamics. *Surveys in Geophysics*, *35*(3), 839–852. https://doi.org/10.1007/s10712-013-9269-4

Beck, H. E., Vergopolan, N., Pan, M., Levizzani, V., van Dijk, A. I. J. M., Weedon, G. P., et al. (2017). Global-scale evaluation of 22 precipitation datasets using gauge observations and hydrological modeling. *Hydrology and Earth System Sciences*, *21*(12), 6201–6217. https://doi.org/10.5194/hess-21-6201-2017

Becker, M., Papa, F., Frappart, F., Alsdorf, D., Calmant, S., da Silva, J. S., et al. (2018). Satellite-based estimates of surface water dynamics in the Congo River Basin. *International Journal of Applied Earth Observation and Geoinformation*, *66*, 196–209. https://doi.org/10.1016/j.jag.2017.11.015

Benveniste, J.-F. C., Nielsen, K., Frappart, F., Papa, F., & Stéphane Calmant, J. (2017). Hydrological applications of satellite Altimetry Rivers, Lakes, Man-Made reservoirs, inundated areas. In *Satellite altimetry over oceans and land surfaces*. CRC Press.

Biancamaria, S., Durand, M., Andreadis, K. M., Bates, P. D., Boone, A., Mognard, N. M., et al. (2011). Assimilation of virtual wide swath altimetry to improve Arctic river modeling. *Remote Sensing of Environment*, *115*(2), 373–381. https://doi.org/10.1016/j.rse.2010.09.008

Bierkens, M. F. P. (2015). Global hydrology 2015: State, trends, and directions. *Water Resources Research*, *51*(7), 4923–4947. https://doi.org/10.1002/2015WR017173

Bjerklie, D. M., Durand, M., Lenoir, J., Dudley, R. W., Birkett, C. M., Jones, J. W., & Harlan, M. (2023). Satellite remote sensing of river discharge: A framework for assessing the accuracy of discharge estimates made from satellite remote sensing observations. *Journal of Applied Remote Sensing*, *17*(1), 014520. https://doi.org/10.1117/1.JRS.17.014520

Blyverket, J., Hamer, P. D., Bertino, L., Albergel, C., Fairbairn, D., & Lahoz, W. A. (2019). An evaluation of the EnKF vs. EnOI and the assimilation of SMAP, SMOS and ESA CCI soil moisture data over the contiguous US. *Remote Sensing*, *11*(5), 478. https://doi.org/10.3390/rs11050478

Boisier, J. P., Ciais, P., Ducharne, A., & Guimberteau, M. (2015). Projected strengthening of Amazonian dry season by constrained climate model simulations. *Nature Climate Change*, *5*(7), 656–660. https://doi.org/10.1038/nclimate2658

Brakenridge, R., & Anderson, E. (2006). Modis-based flood detection, mapping and measurement: The potential for operational hydrological applications. In *Transboundary floods: Reducing risks through flood management* (pp. 1–12). Kluwer Academic Publishers. https://doi.org/10.1007/1-4020-4902-1_1

Brandhorst, N., & Neuweiler, I. (2023). Impact of parameter updates on soil moisture assimilation in a 3D heterogeneous hillslope model. *Hydrology and Earth System Sciences*, *27*(6), 1301–1323. https://doi.org/10.5194/hess-27-1301-2023

Brêda, J. P. L. F., de Paiva, R. C. D., Chou, S. C., & Collischonn, W. (2022). Assessing extreme precipitation from a regional climate model in different spatial–temporal scales: A hydrological perspective in South America. *International Journal of Climatology*, *42*(16), 8904–8927. https://doi.org/10.1002/joc.7782

Brisco, B., Short, N., van der Sanden, J., Landry, R., & Raymond, D. (2009). A semi-automated tool for surface water mapping with RADARSAT-1. *Canadian Journal of Remote Sensing*, *35*(4), 336–344. https://doi.org/10.5589/m09-025

Brivio, P. A., Colombo, R., Maggi, M., & Tomasoni, R. (2002). Integration of remote sensing data and GIS for accurate mapping of flooded areas. *International Journal of Remote Sensing*, *23*(3), 429–441. https://doi.org/10.1080/01431160010014729

Brocca, L., Moramarco, T., Melone, F., Wagner, W., Hasenauer, S., & Hahn, S. (2012). Assimilation of surface- and root-zone ASCAT soil moisture products into rainfall-runoff modeling. *IEEE Transactions on Geoscience and Remote Sensing*, *50*(7 PART1), 2542–2555. https://doi.org/10.1109/TGRS.2011.2177468

Burgers, G., Van Leeuwen, P. J., & Evensen, G. (1998). Analysis scheme in the ensemble Kalman filter. *Monthly Weather Review*, *126*(6), 1719–1724. https://doi.org/10.1175/1520-0493(1998)126<1719:ASITEK>2.0.CO;2

Camporese, M., & Girotto, M. (2022). Recent advances and opportunities in data assimilation for physics-based hydrological modeling. *Frontiers in Water*, *4*, 948832. https://doi.org/10.3389/frwa.2022.948832

Chen, F., Crow, W. T., Starks, P. J., & Moriasi, D. N. (2011). Improving hydrologic predictions of a catchment model via assimilation of surface soil moisture. *Advances in Water Resources*, *34*(4), 526–536. https://doi.org/10.1016/j.advwatres.2011.01.011

Chen, L., & Wang, L. (2018). Recent advance in earth observation big data for hydrology. *Big Earth Data*, *2*(1), 86–107. https://doi.org/10.1080/20964471.2018.1435072

Clark, M. P., Rupp, D. E., Woods, R. A., Zheng, X., Ibbitt, R. P., Slater, A. G., et al. (2008). Hydrological data assimilation with the ensemble Kalman filter: Use of streamflow observations to update states in a distributed hydrological model. *Advances in Water Resources*, *31*(10), 1309–1324. https://doi.org/10.1016/j.advwatres.2008.06.005

CNES. (1996). User handbook merged topex/poseidon products. (July).

Collischonn, W., Allasia, D., da Silva, B. C., & Tucci, C. E. M. (2007). The MGB-IPH model for large-scale rainfall-runoff modelling. *Hydrological Sciences Journal*, *52*(5), 878–895. https://doi.org/10.1623/hysj.52.5.878

Corato, G., Matgen, P., Fenicia, F., Schlaffer, S., & Chini, M. (2014). Assimilating satellite-derived soil moisture products into a distributed hydrological model. In *2014 International Geoscience and Remote Sensing Symposium (IGARSS)* (pp. 3315–3318). IEEE. https://doi.org/10.1109/IGARSS.2014.6947189

Cretaux, J.-F., Calmant, S., Papa, F., Frappart, F., Paris, A., & Berge-Nguyen, M. (2023). Inland surface waters quantity monitored from remote sensing. *Surveys in Geophysics*, *44*(5), 1519–1552. https://doi.org/10.1007/s10712-023-09803-x

Crow, W. T., & Ryu, D. (2008). A new data assimilation approach for improving hydrologic prediction using remotely-sensed soil moisture retrievals. *Hydrology and Earth System Sciences Discussions*, *5*(4), 2005–2044. https://doi.org/10.5194/hessd-5-2005-2008

Crow, W. T., & Wood, E. F. (2003). The assimilation of remotely sensed soil brightness temperature imagery into a land surface model using ensemble Kalman filtering: A case study based on ESTAR measurements during SGP97. *Advances in Water Resources*, *26*(2), 137–149. https://doi.org/10.1016/S0309-1708(02)00088-X

Decharme, B., Alkama, R., Papa, F., Faroux, S., Douville, H., & Prigent, C. (2012). Global off-line evaluation of the ISBA-TRIP flood model. *Climate Dynamics*, *38*(7), 1389–1412. https://doi.org/10.1007/s00382-011-1054-9

De Lannoy, G. J. M., & Reichle, R. H. (2016). Global assimilation of multiangle and multipolarization SMOS brightness temperature observations into the GEOS-5 catchment land surface model for soil moisture estimation. *Journal of Hydrometeorology*, *17*(2), 669–691. https://doi.org/10.1175/JHM-D-15-0037.1

De Paiva, R. C. D., Buarque, D. C., Collischonn, W., Bonnet, M.-P., Frappart, F., Calmant, S., & Bulhões Mendes, C. A. (2013). Large-scale hydrologic and hydrodynamic modeling of the Amazon River basin. *Water Resources Research*, *49*(3), 1226–1243. https://doi.org/10.1002/wrcr.20067

Döll, P., Berkhoff, K., Bormann, H., Fohrer, N., Gerten, D., Hagemann, S., & Krol, M. (2008). Advances and visions in large-scale hydrological modelling: Findings from the 11th workshop on large-scale hydrological modelling. *Advances in Geosciences*, *18*, 51–61. https://doi.org/10.5194/adgeo-18-51-2008

Durand, M., Gleason, C. J., Garambois, P. A., Bjerklie, D., Smith, L. C., Roux, H., et al. (2016). An intercomparison of remote sensing river discharge estimation algorithms from measurements of river height, width, and slope. *Water Resources Research*, *52*(6), 4527–4549. https://doi.org/10.1002/2015WR018434

Emery, C. M., Paris, A., Biancamaria, S., Boone, A., Calmant, S., Garambois, P. A., & Da Silva, J. S. (2018). Large-scale hydrological model river storage and discharge correction using a satellite altimetry-based discharge product. *Hydrology and Earth System Sciences*, *22*(4), 2135–2162. https://doi.org/10.5194/hess-22-2135-2018

Espinoza, J. C., Ronchail, J., Guyot, J. L., Cochonneau, G., Naziano, F., Lavado, W., et al. (2009). Spatio-temporal rainfall variability in the Amazon basin countries (Brazil, Peru, Bolivia, Colombia, and Ecuador). *International Journal of Climatology*, *29*(11), 1574–1594. https://doi.org/10.1002/joc.1791

Espinoza, J. C., Ronchail, J., Guyot, J. L., Junquas, C., Vauchel, P., Lavado, W., et al. (2011). Climate variability and extreme drought in the upper Solimões River (western Amazon Basin): Understanding the exceptional 2010 drought. *Geophysical Research Letters*, *38*(13), 13406. https://doi.org/10.1029/2011GL047862

Espinoza, J. C., Ronchail, J., Marengo, J. A., & Segura, H. (2019a). Contrasting North–South changes in Amazon wet-day and dry-day frequency and related atmospheric features (1981–2017). *Climate Dynamics*, *52*(9–10), 5413–5430. https://doi.org/10.1007/s00382-018-4462-2

Espinoza, J. C., Sörensson, A. A., Ronchail, J., Molina-Carpio, J., Segura, H., Gutierrez-Cori, O., et al. (2019b). Regional hydro-climatic changes in the southern Amazon Basin (upper Madeira basin) during the 1982–2017 period. *Journal of Hydrology: Regional Studies*, *26*(November), 100637. https://doi.org/10.1016/j.ejrh.2019.100637

Evensen, G. (1994). Sequential data assimilation with a nonlinear quasi-geostrophic model using Monte Carlo methods to forecast error statistics. *Journal of Geophysical Research*, *99*(C5), 10143–10162. https://doi.org/10.1029/94jc00572

Evensen, G. (2003). The ensemble Kalman filter: Theoretical formulation and practical implementation. *Ocean Dynamics*, *53*(4), 343–367. https://doi.org/10.1007/s10236-003-0036-9

Evensen, G. (2004). Sampling strategies and square root analysis schemes for the EnKF. *Ocean Dynamics*, *54*(6), 539–560. https://doi.org/10.1007/s10236-004-0099-2

Fassoni-Andrade, A. C., Fleischmann, A. S., Papa, F., de Paiva, R. C. D., Wongchuig, S., Melack, J. M., et al. (2021). Amazon hydrology from space: Scientific advances and future challenges. *Reviews of Geophysics*, *59*(4), e2020RG000728. https://doi.org/10.1029/2020rg000728

Fleischmann, A. S., Papa, F., Fassoni-Andrade, A., Melack, J. M., Wongchuig, S., Paiva, R. C. D., et al. (2022). How much inundation occurs in the Amazon River basin? *Remote Sensing of Environment*, *278*, 113099. https://doi.org/10.1016/j.rse.2022.113099

Fleischmann, A. S., Papa, F., Hamilton, S. K., Fassoni-Andrade, A., Wongchuig, S., Espinoza, J.-C., et al. (2023). Increased floodplain inundation in the Amazon since 1980. *Environmental Research Letters*, *18*(3), 034024. https://doi.org/10.1088/1748-9326/acb9a7

Fossum, K., & Mannseth, T. (2017). Coarse-scale data assimilation as a generic alternative to localization. *Computational Geosciences*, *21*(1), 167–186. https://doi.org/10.1007/s10596-016-9602-3

Frappart, F., Calmant, S., Cauhopé, M., Seyler, F., & Cazenave, A. (2006). Preliminary results of ENVISAT RA-2-derived water levels validation over the Amazon basin. *Remote Sensing of Environment*, *100*(2), 252–264. https://doi.org/10.1016/j.rse.2005.10.027

Frappart, F., Papa, F., Santos Da Silva, J., Ramillien, G., Prigent, C., Seyler, F., & Calmant, S. (2012). Surface freshwater storage and dynamics in the Amazon basin during the 2005 exceptional drought. *Environmental Research Letters*, *7*(4), 044010. https://doi.org/10.1088/1748-9326/7/4/044010

Funk, C., Peterson, P., Landsfeld, M., Pedreros, D., Verdin, J., Shukla, S., et al. (2015). The climate hazards infrared precipitation with stations - a new environmental record for monitoring extremes. *Scientific Data*, *2*, 1–21. https://doi.org/10.1038/sdata.2015.66

Garambois, P. A., Calmant, S., Roux, H., Paris, A., Monnier, J., Finaud-Guyot, P., et al. (2017). Hydraulic visibility: Using satellite altimetry to parameterize a hydraulic model of an ungauged reach of a braided river. *Hydrological Processes*, *31*(4), 756–767. https://doi.org/10.1002/hyp.11033

García-Alén, G., Hostache, R., Cea, L., & Puertas, J. (2023). Joint assimilation of satellite soil moisture and streamflow data for the hydrological application of a two-dimensional shallow water model. *Journal of Hydrology*, *621*, 129667. https://doi.org/10.1016/j.jhydrol.2023.129667

Gaspari, G., & Cohn, S. E. (1999). Construction of correlation functions in two and three dimensions. *Quarterly Journal of the Royal Meteorological Society*, *125*(554), 723–757. https://doi.org/10.1256/smsqj.55416

Gavahi, K., Abbaszadeh, P., & Moradkhani, H. (2022). How does precipitation data influence the land surface data assimilation for drought monitoring? *The Science of the Total Environment*, *831*, 154916. https://doi.org/10.1016/j.scitotenv.2022.154916

Gavahi, K., Abbaszadeh, P., Moradkhani, H., Zhan, X., & Hain, C. (2020). Multivariate assimilation of remotely sensed soil moisture and evapotranspiration for drought monitoring. *Journal of Hydrometeorology*, *21*(10), 2293–2308. https://doi.org/10.1175/JHM-D-20-0057.1

Getirana, A., Peters-Lidard, C., Rodell, M., & Bates, P. D. (2017). Trade-off between cost and accuracy in large-scale surface water dynamic modeling. *Water Resources Research*, *53*(6), 4942–4955. https://doi.org/10.1002/2017WR020519

Gichamo, T. Z., Popescu, I., Jonoski, A., & Solomatine, D. (2012). River cross-section extraction from the ASTER global DEM for flood modeling. *Environmental Modelling and Software*, *31*, 37–46. https://doi.org/10.1016/j.envsoft.2011.12.003

Girotto, M., Reichle, R. H., Rodell, M., Liu, Q., Mahanama, S., & De Lannoy, G. J. M. (2019). Multi-sensor assimilation of SMOS brightness temperature and GRACE terrestrial water storage observations for soil moisture and shallow groundwater estimation. *Remote Sensing of Environment*, *227*, 12–27. https://doi.org/10.1016/j.rse.2019.04.001

Gloor, M., Brienen, R. J. W., Galbraith, D., Feldpausch, T. R., Schöngart, J., Guyot, J.-L., et al. (2013). Intensification of the Amazon hydrological cycle over the last two decades. *Geophysical Research Letters*, *40*(9), 1729–1733. https://doi.org/10.1002/grl.50377

Gudmundsson, L., Leonard, M., Do, H. X., Westra, S., & Seneviratne, S. I. (2019). Observed trends in global indicators of mean and extreme streamflow. *Geophysical Research Letters*, *46*(2), 756–766. https://doi.org/10.1029/2018GL079725

Guimberteau, M., Ronchail, J., Espinoza, J. C., Lengaigne, M., Sultan, B., Polcher, J., et al. (2013). Future changes in precipitation and impacts on extreme streamflow over Amazonian sub-basins. *Environmental Research Letters*, *8*(1), 014035. https://doi.org/10.1088/1748-9326/8/1/014035

Güntner, A. (2008). Improvement of global hydrological models using GRACE data. *Surveys in Geophysics*, *29*(4–5), 375–397. https://doi.org/10.1007/s10712-008-9038-y

Hamill, T. M., Whitaker, J. S., & Snyder, C. (2001). Distance-dependent filtering of background error covariance estimates in an ensemble Kalman filter. *Monthly Weather Review*, *129*(11), 2776–2790. https://doi.org/10.1175/1520-0493(2001)129<2776:DDFOBE>2.0.CO;2

Hess, L. L., Melack, J. M., Affonso, A. G., Barbosa, C., Gastil-Buhl, M., & Novo, E. M. L. M. (2015). Wetlands of the lowland Amazon Basin: Extent, vegetative cover, and Dual-season inundated area as mapped with JERS-1 synthetic aperture radar. *Wetlands*, *35*(4), 745–756. https://doi.org/10.1007/s13157-015-0666-y

Houtekamer, P. L., & Mitchell, H. L. (2001). A sequential ensemble Kalman filter for atmospheric data assimilation. *Monthly Weather Review*, *129*(1), 123–137. https://doi.org/10.1175/1520-0493(2001)129<0123:ASEKFF>2.0.CO;2

Houtekamer, P. L., & Mitchell, H. L. (2006). Ensemble Kalman filtering. *Quarterly Journal of the Royal Meteorological Society*, *131*(613), 3269–3289. https://doi.org/10.1256/qj.05.135

Kauffeldt, A., Wetterhall, F., Pappenberger, F., Salamon, P., & Thielen, J. (2016). Technical review of large-scale hydrological models for implementation in operational flood forecasting schemes on continental level. *Environmental Modelling & Software*, *75*, 68–76. https://doi.org/10.1016/j.envsoft.2015.09.009

Kerr, Y., Waldteufel, P., Wigneron, J.-P., Boutin, J., Reul, N., Bitar, A. A., et al. (2012). The soil moisture and Ocean Salinity (SMOS) mission: First results and achievements. *Revue Française de Photogrammétrie et de Télédétection*, (200), 12–19. https://doi.org/10.52638/rfpt.2012.57

Kerr, Y. H., Waldteufel, P., Wigneron, J.-P., Martinuzzi, J., Font, J., & Berger, M. (2001). Soil moisture retrieval from space: The soil moisture and Ocean Salinity (SMOS) mission. *IEEE Transactions on Geoscience and Remote Sensing*, *39*(8), 1729–1735. https://doi.org/10.1109/36.942551

Khaki, M., Forootan, E., Kuhn, M., Awange, J., Papa, F., & Shum, C. K. (2018). A study of Bangladesh's sub-surface water storages using satellite products and data assimilation scheme. *Science of the Total Environment*, *625*, 963–977. https://doi.org/10.1016/j.scitotenv.2017.12.289

Khaki, M., Hendricks Franssen, H. J., & Han, S. C. (2020). Multi-mission satellite remote sensing data for improving land hydrological models via data assimilation. *Scientific Reports*, *10*(1), 1–23. https://doi.org/10.1038/s41598-020-75710-5

Khaki, M., Hoteit, I., Kuhn, M., Awange, J., Forootan, E., van Dijk, A. I. J. M., et al. (2017). Assessing sequential data assimilation techniques for integrating GRACE data into a hydrological model. *Advances in Water Resources*, *107*, 301–316. https://doi.org/10.1016/j.advwatres.2017.07.001

Khaki, M., Hoteit, I., Kuhn, M., Forootan, E., & Awange, J. (2019). Assessing data assimilation frameworks for using multi-mission satellite products in a hydrological context. *The Science of the Total Environment*, *647*(October 2017), 1031–1043. https://doi.org/10.1016/j.scitotenv.2018.08.032

Kitambo, B., Papa, F., Paris, A., Tshimanga, R. M., Calmant, S., Fleischmann, A. S., et al. (2022). A combined use of in situ and satellite-derived observations to characterize surface hydrology and its variability in the Congo River basin. *Hydrology and Earth System Sciences*, *26*(7), 1857–1882. https://doi.org/10.5194/hess-26-1857-2022

Kitambo, B. M., Papa, F., Paris, A., Tshimanga, R. M., Frappart, F., Calmant, S., et al. (2023). A long-term monthly surface water storage dataset for the Congo basin from 1992 to 2015. *Earth System Science Data*, *15*(7), 2957–2982. https://doi.org/10.5194/essd-15-2957-2023

Kittel, C., Nielsen, K., Tøttrup, C., & Bauer-Gottwein, P. (2018). Informing a hydrological model of the Ogooué with multi-mission remote sensing data. *Hydrology and Earth System Sciences*, *22*(2), 1453–1472. https://doi.org/10.5194/hess-22-1453-2018

Koblinsky, C. J., Clarke, R. T., Brenner, A. C., & Frey, H. (1993). Measurement of river level variations with satellite altimetry. *Water Resources Research*, *29*(6), 1839–1848. https://doi.org/10.1029/93WR00542

Kumar, S. V., Jasinski, M., Mocko, D. M., Rodell, M., Borak, J., Li, B., et al. (2019). NCA-LDAS land analysis: Development and performance of a multisensor, multivariate land data assimilation system for the national climate assessment. *Journal of Hydrometeorology*, *20*(8), 1571–1593. https://doi.org/10.1175/JHM-D-17-0125.1

Kumar, S. V., Peters-Lidard, C. D., Santanello, J. A., Reichle, R. H., Draper, C. S., Koster, R. D., et al. (2015). Evaluating the utility of satellite soil moisture retrievals over irrigated areas and the ability of land data assimilation methods to correct for unmodeled processes. *Hydrology and Earth System Sciences*, *19*(11), 4463–4478. https://doi.org/10.5194/hess-19-4463-2015

Kuppel, S., Soulsby, C., Maneta, M. P., & Tetzlaff, D. (2017). Information footprint of different ecohydrological data sources: Using multi-objective calibration of a physically-based model as hypothesis testing. In *AGU fall meeting abstracts* (Vol. 2017, p. H51F–H1334). AA (Northern Rivers Institute, University of Aberdeen, Aberdeen, United Kingdom), AB(School of Geosciences, University of Aberdeen, Aberdeen, United Kingdom), AC(University of Montana, Missoula, MT, United States), AD(Humboldt University of Berlin, Berlin.

Lai, X., Liang, Q., Yesou, H., & Daillet, S. (2014). Variational assimilation of remotely sensed flood extents using a 2-D flood model. *Hydrology and Earth System Sciences*, *18*(11), 4325–4339. https://doi.org/10.5194/hess-18-4325-2014

Landerer, F. W., & Swenson, S. C. (2012). Accuracy of scaled GRACE terrestrial water storage estimates. *Water Resources Research*, *48*(4). https://doi.org/10.1029/2011WR011453

Laraque, A., N'kaya, G. D. M., Orange, D., Tshimanga, R., Tshitenge, J. M., Mahe, G., et al. (2020). Recent budget of hydroclimatology and hydrosedimentology of the Congo river in central Africa. *Water*, *12*(9), 2613. https://doi.org/10.3390/w12092613

Lee, H., Jung, H. C., Yuan, T., Beighley, R. E., & Duan, J. (2014). Controls of terrestrial water storage changes over the Central Congo basin determined by integrating PALSAR ScanSAR. *Envisat Altimetry, and GRACE Data*, 115–129. https://doi.org/10.1002/9781118872086.ch7

Lee, H., Seo, D.-J., & Koren, V. (2011). Assimilation of streamflow and in situ soil moisture data into operational distributed hydrologic models: Effects of uncertainties in the data and initial model soil moisture states. *Advances in Water Resources*, *34*(12), 1597–1615. https://doi.org/10.1016/j.advwatres.2011.08.012

Leon, J. G., Calmant, S., Seyler, F., Bonnet, M.-P., Cauhopé, M., Frappart, F., et al. (2006). Rating curves and estimation of average water depth at the upper Negro River based on satellite altimeter data and modeled discharges. *Journal of Hydrology*, *328*(3–4), 481–496. https://doi.org/10.1016/j.jhydrol.2005.12.006

Lettenmaier, D. P. (2017). Observational breakthroughs lead the way to improved hydrological predictions. *Water Resources Research*, *53*(4), 2591–2597. https://doi.org/10.1002/2017WR020896

Lettenmaier, D. P., & Famiglietti, J. S. (2006). Water from on high. *Nature*, *444*(7119), 562–563. https://doi.org/10.1038/444562a

Lievens, H., Martens, B., Verhoest, N. E. C., Hahn, S., Reichle, R. H., & Miralles, D. G. (2017a). Assimilation of global radar backscatter and radiometer brightness temperature observations to improve soil moisture and land evaporation estimates. *Remote Sensing of Environment*, *189*, 194–210. https://doi.org/10.1016/j.rse.2016.11.022

Lievens, H., Reichle, R. H., Liu, Q., De Lannoy, G. J. M., Dunbar, R. S., Kim, S. B., et al. (2017b). Joint Sentinel-1 and SMAP data assimilation to improve soil moisture estimates. *Geophysical Research Letters*, *44*(12), 6145–6153. https://doi.org/10.1002/2017GL073904

Liu, Y., & Gupta, H. V. (2007). Uncertainty in hydrologic modeling: Toward an integrated data assimilation framework. *Water Resources Research*, *43*(7), 1–18. https://doi.org/10.1029/2006WR005756

Liu, Y., Weerts, A. H., Clark, M., Hendricks Franssen, H. J., Kumar, S., Moradkhani, H., et al. (2012). Advancing data assimilation in operational hydrologic forecasting: Progresses, challenges, and emerging opportunities. *Hydrology and Earth System Sciences*, *16*(10), 3863–3887. https://doi.org/10.5194/hess-16-3863-2012

López, P. L., Sutanudjaja, E. H., Schellekens, J., Sterk, G., & Bierkens, M. F. P. (2017). Calibration of a large-scale hydrological model using satellite-based soil moisture and evapotranspiration products. *Hydrology and Earth System Sciences*, *21*(6), 3125–3144. https://doi.org/10.5194/hess-21-3125-2017

Loukas, A., & Vasiliades, L. (2014). Streamflow simulation methods for ungauged and poorly gauged watersheds. *Natural Hazards and Earth System Sciences*, *14*(7), 1641–1661. https://doi.org/10.5194/nhess-14-1641-2014

Marengo, J. A. (2005). Characteristics and spatio-temporal variability of the Amazon River basin water budget. *Climate Dynamics*, *24*(1), 11–22. https://doi.org/10.1007/s00382-004-0461-6

Marengo, J. A., Borma, L. S., Rodriguez, D. A., Pinho, P., Soares, W. R., & Alves, L. M. (2013). Recent extremes of drought and flooding in Amazonia: Vulnerabilities and human adaptation. *American Journal of Climate Change*, *02*(02), 87–96. https://doi.org/10.4236/ajcc.2013.22009

Marengo, J. A., & Espinoza, J. C. (2016). Extreme seasonal droughts and floods in Amazonia: Causes, trends and impacts. *International Journal of Climatology*, *36*(3), 1033–1050. https://doi.org/10.1002/joc.4420

Massari, C., Brocca, L., Tarpanelli, A., & Moramarco, T. (2015). Data assimilation of satellite soil moisture into rainfall-runoffmodelling: A complex recipe? *Remote Sensing*, *7*(9), 11403–11433. https://doi.org/10.3390/rs70911403

Melesse, A. M., Weng, Q., Thenkabail, P. S., & Senay, G. B. (2007). Remote sensing sensors and applications in environmental resources mapping and modelling. *Sensors*, *7*(12), 3209–3241. https://doi.org/10.3390/s7123209

Michailovsky, C. I., Milzow, C., & Bauer-Gottwein, P. (2013). Assimilation of radar altimetry to a routing model of the Brahmaputra River. *Water Resources Research*, *49*(8), 4807–4816. https://doi.org/10.1002/wrcr.20345

Miguez-Macho, G., & Fan, Y. (2012). The role of groundwater in the Amazon water cycle: 1. Influence on seasonal streamflow, flooding and wetlands: Amazon groundwater-surface water link. *Journal of Geophysical Research*, *117*(D15). https://doi.org/10.1029/2012JD017539

Milly, P. C. D., Dunne, K. A., & Vecchia, A. V. (2005). Global pattern of trends in streamflow and water availability in a changing climate. *Nature*, *438*(7066), 347–350. https://doi.org/10.1038/nature04312

Molinier, M., Guyot, J. L., De Oliveira, E., & Guimaraes, V. (1996). *Les regimes hydrologiques de l'Amazone et de ses affluents* (Vol. 238, pp. 209–222). IAHS-AISH Publication.

Montzka, C., Pauwels, V. R. N., Franssen, H. J. H., Han, X., & Vereecken, H. (2012). Multivariate and multiscale data assimilation in terrestrial systems: A review. *Sensors*, *12*, 16333. https://doi.org/10.3390/s121216291

Moody, J. A., & Troutman, B. M. (2002). Characterization of the spatial variability of channel morphology. *Earth Surface Processes and Landforms*, *27*(12), 1251–1266. https://doi.org/10.1002/esp.403

Moradkhani, H., Sorooshian, S., Gupta, H. V., & Houser, P. R. (2005). Dual state-parameter estimation of hydrological models using ensemble Kalman filter. *Advances in Water Resources*, *28*(2), 135–147. https://doi.org/10.1016/j.advwatres.2004.09.002

Musuuza, J. L., Gustafsson, D., Pimentel, R., Crochemore, L., & Pechlivanidis, I. (2020). Impact of satellite and in situ data assimilation on hydrological predictions. *Remote Sensing*, *12*(5), 11–13. https://doi.org/10.3390/rs12050811

Nair, A. S., Mangla, R., Thiruvengadam, P., & Indu, J. (2020). Remote sensing data assimilation. *Hydrological Sciences Journal*, *0*(0), 1. https://doi.org/10.1080/02626667.2020.1761021

New, M., Lister, D., Hulme, M., & Makin, I. (2002). A high-resolution data set of surface climate over global land areas. *Climate Research*, *21*(1), 1–25. https://doi.org/10.3354/cr021001

Nijssen, B., & Lettenmaier, D. P. (2004). Effect of precipitation sampling error on simulated hydrological fluxes and states: Anticipating the Global Precipitation Measurement satellites. *Journal of Geophysical ResearchD: Atmosphere*, *109*(2), 1–15. https://doi.org/10.1029/2003jd003497

Nijzink, R. C., Almeida, S., Pechlivanidis, I. G., Capell, R., Gustafssons, D., Arheimer, B., et al. (2018). Constraining conceptual hydrological models with multiple information sources. *Water Resources Research*, *54*(10), 8332–8362. https://doi.org/10.1029/2017WR021895

Oliveira, A. M., Fleischmann, A. S., & Paiva, R. C. D. (2021). On the contribution of remote sensing-based calibration to model hydrological and hydraulic processes in tropical regions. *Journal of Hydrology*, *597*, 126184. https://doi.org/10.1016/j.jhydrol.2021.126184

O'Loughlin, F. E., Paiva, R. C. D., Durand, M., Alsdorf, D. E., & Bates, P. D. (2016). A multi-sensor approach towards a global vegetation corrected SRTM DEM product. *Remote Sensing of Environment*, *182*, 49–59. https://doi.org/10.1016/j.rse.2016.04.018

Paca, V. H. M., Espinoza-Dávalos, G. E., Hessels, T. M., Moreira, D. M., Comair, G. F., & Bastiaanssen, W. G. M. (2019). The spatial variability of actual evapotranspiration across the Amazon River Basin based on remote sensing products validated with flux towers. *Ecological Processes*, *8*(1), 6. https://doi.org/10.1186/s13717-019-0158-8

Paiva, R. C. D., Collischonn, W., Bonnet, M.-P., de Gonçalves, L. G. G., Calmant, S., Getirana, A., & Santos da Silva, J. (2013). Assimilating in situ and radar altimetry data into a large-scale hydrologic-hydrodynamic model for streamflow forecast in the Amazon. *Hydrology and Earth System Sciences*, *17*(7), 2929–2946. https://doi.org/10.5194/hess-17-2929-2013

Panzeri, M., Riva, M., Guadagnini, A., & Neuman, S. P. (2013). Data assimilation and parameter estimation via ensemble Kalman filter coupled with stochastic moment equations of transient groundwater flow. *Water Resources Research*, *49*(3), 1334–1344. https://doi.org/10.1002/wrcr.20113

Papa, F., Crétaux, J.-F., Grippa, M., Robert, E., Trigg, M., Tshimanga, R. M., et al. (2022). Water resources in Africa under global change: Monitoring surface waters from space. *Surveys in Geophysics*, *44*(1), 43–93. https://doi.org/10.1007/s10712-022-09700-9

Papa, F., Frappart, F., Malbeteau, Y., Shamsudduha, M., Vuruputur, V., Sekhar, M., et al. (2015). Satellite-derived surface and sub-surface water storage in the Ganges–Brahmaputra River Basin. *Journal of Hydrology: Regional Studies*, *4*, 15–35. https://doi.org/10.1016/j.ejrh.2015.03.004

Papa, F., Prigent, C., Aires, F., Jimenez, C., Rossow, W. B., & Matthews, E. (2010). Interannual variability of surface water extent at the global scale, 1993-2004. *Journal of Geophysical Research*, *115*(12), 1–17. https://doi.org/10.1029/2009JD012674

Paris, A., Calmant, S., Gosset, M., Fleischmann, A. S., Conchy, T. S. X., Garambois, P., et al. (2022). Monitoring hydrological variables from remote sensing and modeling in the Congo River Basin. In R. M. Tshimanga, G. D. M. N'kaya, & D. Alsdorf (Eds.), *Geophysical monograph series* (1st ed., pp. 339–366). Wiley. https://doi.org/10.1002/9781119657002.ch18

Paris, A., Dias de Paiva, R., Santos da Silva, J., Medeiros Moreira, D., Calmant, S., Garambois, P.-A., et al. (2016). Stage-discharge rating curves based on satellite altimetry and modeled discharge in the Amazon basin. *Water Resources Research*, *52*(5), 3787–3814. https://doi.org/10.1002/2014WR016618

Pathiraja, S., Marshall, L., Sharma, A., & Moradkhani, H. (2016). Hydrologic modeling in dynamic catchments: A data assimilation approach. *Water Resources Research*, *52*(5), 3350–3372. https://doi.org/10.1002/2015WR017192

Pekel, J. F., Cottam, A., Gorelick, N., & Belward, A. S. (2016). High-resolution mapping of global surface water and its long-term changes. *Nature*, *540*(7633), 418–422. https://doi.org/10.1038/nature20584

Pham-Duc, B., Prigent, C., & Aires, F. (2017). One-year monitoring of surface waters within Cambodia and the Vietnamese Mekong delta with SAR Sentinel-1 observations. *Water*, *9*(6), 366. https://doi.org/10.3390/w9060366

Pietroniro, A., & Prowse, T. D. (2002). Applications of remote sensing in hydrology. *Hydrological Processes*, *16*(8), 1537–1541. https://doi.org/10.1002/hyp.1018

Pimentel, R., Crochemore, L., Andersson, J. C. M., & Arheimer, B. (2023). Assessing robustness in global hydrological predictions by comparing modelling and Earth observations. *Hydrological Sciences Journal*, *0*(0), 1–16. https://doi.org/10.1080/02626667.2023.2267544

Pontes, P. R. M., Fan, F. M., Fleischmann, A. S., de Paiva, R. C. D., Buarque, D. C., Siqueira, V. A., et al. (2017). MGB-IPH model for hydrological and hydraulic simulation of large floodplain river systems coupled with open source GIS. *Environmental Modelling & Software*, *94*, 1–20. https://doi.org/10.1016/j.envsoft.2017.03.029

Prigent, C., Jimenez, C., & Bousquet, P. (2020). Satellite-derived global surface water extent and dynamics over the last 25 Years (GIEMS-2). *Journal of Geophysical Research: Atmospheres*, *125*(3), e2019JD030711. https://doi.org/10.1029/2019JD030711

Prigent, C., Papa, F., Aires, F., Jimenez, C., Rossow, W. B., & Matthews, E. (2012). Changes in land surface water dynamics since the 1990s and relation to population pressure. *Geophysical Research Letters*, *39*(8), 2–6. https://doi.org/10.1029/2012GL051276

Prigent, C., Papa, F., Aires, F., Rossow, W. B., & Matthews, E. (2007). Global inundation dynamics inferred from multiple satellite observations, 1993-2000. *Journal of Geophysical Research*, *112*(12), 1993–2000. https://doi.org/10.1029/2006JD007847

Rajib, M. A., Merwade, V., & Yu, Z. (2016). Multi-objective calibration of a hydrologic model using spatially distributed remotely sensed/in-situ soil moisture. *Journal of Hydrology*, *536*, 192–207. https://doi.org/10.1016/j.jhydrol.2016.02.037

Ramillien, G., Famiglietti, J. S., & Wahr, J. (2008). Detection of continental hydrology and glaciology signals from GRACE: A review. *Surveys in Geophysics*, *29*(4–5), 361–374. https://doi.org/10.1007/s10712-008-9048-9

Reager, J. T., & Famiglietti, J. S. (2009). Global terrestrial water storage capacity and flood potential using GRACE. *Geophysical Research Letters*, *36*(23), 2–7. https://doi.org/10.1029/2009GL040826

Reichle, R. H. (2008). Data assimilation methods in the Earth sciences. *Advances in Water Resources*, *31*(11), 1411–1418. https://doi.org/10.1016/j.advwatres.2008.01.001

Reichle, R. H., McLaughlin, D. B., & Entekhabi, D. (2002). Hydrologic data assimilation with the ensemble Kalman filter. *Monthly Weather Review*, *130*(1), 103–114. https://doi.org/10.1175/1520-0493(2002)130<0103:HDAWTE>2.0.CO;2

Revel, M., Zhou, X., Yamazaki, D., & Kanae, S. (2023). Assimilation of transformed water surface elevation to improve river discharge estimation in a continental-scale river. *Hydrology and Earth System Sciences*, *27*(3), 647–671. https://doi.org/10.5194/hess-27-647-2023

Revilla-Romero, B., Wanders, N., Burek, P., Salamon, P., & de Roo, A. (2016). Integrating remotely sensed surface water extent into continental scale hydrology. *Journal of Hydrology*, *543*, 659–670. https://doi.org/10.1016/j.jhydrol.2016.10.041

Rodell, M., & Famiglietti, J. S. (2001). An analysis of terrestrial water storage variations in Illinois with implications for the Gravity Recovery and Climate Experiment (GRACE). *Water Resources Research*, *37*(5), 1327–1339. https://doi.org/10.1029/2000WR900306

Rodell, M., & Famiglietti, J. S. (2002). The potential for satellite-based monitoring of groundwater storage changes using GRACE: The High Plains aquifer, Central US. *Journal of Hydrology*, *263*(1–4), 245–256. https://doi.org/10.1016/S0022-1694(02)00060-4

Rosenqvist, Å., Forsberg, B. R., Pimentel, T., Rauste, Y. A., & Richey, J. E. (2002). The use of spaceborne radar data to model inundation patterns and trace gas emissions in the central Amazon floodplain. *International Journal of Remote Sensing*, *23*(7), 1303–1328. https://doi.org/10.1080/01431160110092911

Rosenqvist, A., Shimada, M., & Watanabe, M. (2004). Alos PALSAR: Technical outline and mission concepts. *International Symposium on Retrieval of Bio- and Geophysical Parameters from SAR Data for Land Applications*, *1*(7), 1–7.

Roux, E., Cauhope, M., Bonnet, M. P., Calmant, S., Vauchel, P., & Seyler, F. (2008). Daily water stage estimated from satellite altimetric data for large river basin monitoring. *Hydrological Sciences Journal*, *53*(1), 81–99. https://doi.org/10.1623/hysj.53.1.81

Saleska, S. R., da Rrocha, H. R., Huete, A. R., Nobre, A. D., Artaxo, P., & Shimabukuro, Y. E. (2013). *LBA-ECO CD-32 flux tower network data compilation* (pp. 1999–2006). Brazilian Amazon. 267.05443 MB. https://doi.org/10.3334/ORNLDAAC/1174

Sandholt, I., Andersen, J., Dybkjær, G., Lo, M., Rasmussen, K., Refsgaard, J. C., & Høgh-Jensen, K. (1999). Use of remote sensing data in distributed hydrological models: Applications in the Senegal River basin. *Geografisk Tidsskrift-Danish Journal of Geography*, *99*(1), 47–57. https://doi.org/10.1080/00167223.1999.10649422

Scanlon, B. R., Zhang, Z., Save, H., Wiese, D. N., Landerer, F. W., Long, D., et al. (2016). Global evaluation of new GRACE mascon products for hydrologic applications. *Water Resources Research*, *52*(12), 9412–9429. https://doi.org/10.1002/2016WR019494

Schmugge, T. J., Kustas, W. P., Ritchie, J. C., Jackson, T. J., & Rango, A. (2002). Remote sensing in hydrology. *Advances in Water Resources*, *25*(8–12), 1367–1385. https://doi.org/10.1016/S0309-1708(02)00065-9

Schneider, R., Nygaard Godiksen, P., Villadsen, H., Madsen, H., & Bauer-Gottwein, P. (2017). Application of CryoSat-2 altimetry data for river analysis and modelling. *Hydrology and Earth System Sciences*, *21*(2), 751–764. https://doi.org/10.5194/hess-21-751-2017

Schneider, R., Ridler, M. E., Godiksen, P. N., Madsen, H., & Bauer-Gottwein, P. (2018). A data assimilation system combining CryoSat-2 data and hydrodynamic river models. *Journal of Hydrology*, *557*, 197–210. https://doi.org/10.1016/j.jhydrol.2017.11.052

Shi, Y., Davis, K. J., Zhang, F., Duffy, C. J., & Yu, X. (2014). Parameter estimation of a physically based land surface hydrologic model using the ensemble Kalman filter: A synthetic experiment. *Water Resources Research*, *50*(1), 706–724. https://doi.org/10.1002/2013WR014070

Shokri, A., Walker, J. P., van Dijk, A. I. J. M., & Pauwels, V. R. N. (2018). Performance of different ensemble Kalman filter structures to assimilate GRACE terrestrial water storage estimates into a high-resolution hydrological model: A synthetic study. *Water Resources Research*, *54*(11), 8931–8951. https://doi.org/10.1029/2018WR022785

Silva, J. S. D., Calmant, S., Seyler, F., Rotunno Filho, O. C., Cochonneau, G., & Mansur, W. J. (2010). Water levels in the Amazon basin derived from the ERS 2 and ENVISAT radar altimetry missions. *Remote Sensing of Environment*, *114*(10), 2160–2181. https://doi.org/10.1016/j.rse.2010.04.020

Silvestro, F., Gabellani, S., Rudari, R., Delogu, F., Laiolo, P., & Boni, G. (2015). Uncertainty reduction and parameter estimation of a distributed hydrological model with ground and remote-sensing data. *Hydrology and Earth System Sciences*, *19*(4), 1727–1751. https://doi.org/10.5194/hess-19-1727-2015

Siqueira, V. A., Paiva, R. C. D., Fleischmann, A. S., Fan, F. M., Ruhoff, A. L., Pontes, P. R. M., et al. (2018). Toward continental hydrologic-hydrodynamic modeling in South America. *Hydrology and Earth System Sciences*, *22*(9), 4815–4842. https://doi.org/10.5194/hess-22-4815-2018

Smith, L. C. (1997). Satellite remote sensing of river inundation area, stage, and discharge: A review. *Hydrological Processes*, *11*(10), 1427–1439. https://doi.org/10.1002/(SICI)1099-1085(199708)11:10<1427::AID-HYP473>3.3.CO;2-J

Sood, A., & Smakhtin, V. (2015). Global hydrological models: A review. *Hydrological Sciences Journal*, *60*(4), 549–565. https://doi.org/10.1080/02626667.2014.950580

Sorribas, M. V., Paiva, R. C. D., Melack, J. M., Bravo, J. M., Jones, C., Carvalho, L., et al. (2016). Projections of climate change effects on discharge and inundation in the Amazon basin. *Climatic Change*, *136*(3–4), 555–570. https://doi.org/10.1007/s10584-016-1640-2

Sperna Weiland, F. C., Vrugt, J. A., van Beek, R. L. P. H., Weerts, A. H., & Bierkens, M. F. P. (2015). Significant uncertainty in global scale hydrological modeling from precipitation data errors. *Journal of Hydrology*, *529*, 1095–1115. https://doi.org/10.1016/j.jhydrol.2015.08.061

Stammer, D., & Cazenave, A. (2017). Satellite altimetry over oceans and land surfaces. In D. Stammer & A. Cazenave (Eds.), *Satellite altimetry over oceans and land surfaces*. CRC Press. https://doi.org/10.1201/9781315151779

Strassberg, G., Scanlon, B. R., & Chambers, D. (2009). Evaluation of groundwater storage monitoring with the GRACE satellite: Case study of the High Plains aquifer, central United States. *Water Resources Research*, *45*(5), 1–10. https://doi.org/10.1029/2008WR006892

Su, Z., Fernández-Prieto, D., Timmermans, J., Chen, X., Hungershoefer, K., Roebeling, R., et al. (2014). First results of the earth observation water cycle multi-mission observation strategy (WACMOS). *International Journal of Applied Earth Observation and Geoinformation*, *26*(1), 270–285. https://doi.org/10.1016/j.jag.2013.08.002

Sulistioadi, Y. B., Tseng, K. H., Shum, C. K., Hidayat, H., Sumaryono, M., Suhardiman, A., et al. (2015). Satellite radar altimetry for monitoring small rivers and lakes in Indonesia. *Hydrology and Earth System Sciences*, *19*(1), 341–359. https://doi.org/10.5194/hess-19-341-2015

Sun, Q., Miao, C., Duan, Q., Ashouri, H., Sorooshian, S., & Hsu, K. (2018). A review of global precipitation data sets: Data sources, estimation, and intercomparisons. *Reviews of Geophysics*, *56*(1), 79–107. https://doi.org/10.1002/2017RG000574

Tang, Q., Gao, H., Lu, H., & Lettenmaier, D. P. (2009). Remote sensing: Hydrology. *Progress in Physical Geography*, *33*(4), 490–509. https://doi.org/10.1177/0309133309346650

Tangdamrongsub, N., Han, S., Yeo, I., Dong, J., Steele-dunne, S. C., Willgoose, G., & Walker, J. P. (2020). Advances in water resources multivariate data assimilation of GRACE, SMOS, SMAP measurements for improved regional soil moisture and groundwater storage estimates. *Advances in Water Resources*, *135*(April 2019), 103477. https://doi.org/10.1016/j.advwatres.2019.103477

Tangdamrongsub, N., Steele-Dunne, S. C., Gunter, B. C., Ditmar, P. G., & Weerts, A. H. (2015). Data assimilation of GRACE terrestrial water storage estimates into a regional hydrological model of the Rhine River basin. *Hydrology and Earth System Sciences*, *19*(4), 2079–2100. https://doi.org/10.5194/hess-19-2079-2015

Tapiador, F. J., Turk, F. J., Petersen, W., Hou, A. Y., García-Ortega, E., Machado, L. A. T., et al. (2012). Global precipitation measurement: Methods, datasets and applications. *Atmospheric Research*, *104–105*, 70–97. https://doi.org/10.1016/j.atmosres.2011.10.021

Tapley, B. D., Bettadpur, S., Ries, J. C., Thompson, P. F., & Watkins, M. M. (2004). GRACE measurements of mass variability in the Earth system. *Science*, *305*(5683), 503–505. https://doi.org/10.1126/science.1099192

Tarpanelli, A., Brocca, L., Melone, F., & Moramarco, T. (2013). Hydraulic modelling calibration in small rivers by using coarse resolution synthetic aperture radar imagery. *Hydrological Processes*, *27*(9), 1321–1330. https://doi.org/10.1002/hyp.9550

Tarpanelli, A., Iodice, F., Brocca, L., Restano, M., & Benveniste, J. (2020). River flow monitoring by sentinel-3 OLCI and MODIS: Comparison and combination. *Remote Sensing*, *12*(23), 3867. https://doi.org/10.3390/rs12233867

Tarpanelli, A., Paris, A., Sichangi, A. W., O`Loughlin, F., & Papa, F. (2022). Water resources in Africa: The role of earth observation data and hydrodynamic modeling to derive river discharge. *Surveys in Geophysics*, *44*(1), 97–122. https://doi.org/10.1007/s10712-022-09744-x

Thomas, R. F., Kingsford, R. T., Lu, Y., & Hunter, S. J. (2011). Landsat mapping of annual inundation (1979-2006) of the Macquarie Marshes in semi-arid Australia. *International Journal of Remote Sensing*, *32*(16), 4545–4569. https://doi.org/10.1080/01431161.2010.489064

Tian, X., Xie, Z., Dai, A., Jia, B., & Shi, C. (2010). A microwave land data assimilation system: Scheme and preliminary evaluation over China. *Journal of Geophysical Research*, *115*(21), 1–13. https://doi.org/10.1029/2010JD014370

Tian, Y., Huffman, G. J., Adler, R. F., Tang, L., Sapiano, M., Maggioni, V., & Wu, H. (2013). Modeling errors in daily precipitation measurements: Additive or multiplicative? *Geophysical Research Letters*, *40*(10), 2060–2065. https://doi.org/10.1002/grl.50320

Todini, E. (1996). The ARNO rainfall—Runoff model. *Journal of Hydrology*, *175*(1), 339–382. https://doi.org/10.1016/S0022-1694(96)80016-3

Townsend, P. A. (2002). Relationships between forest structure and the detection of flood inundation in forested wetlands using C-band SAR. *International Journal of Remote Sensing*, *23*(3), 443–460. https://doi.org/10.1080/01431160010014738

Trudel, M., Leconte, R., & Paniconi, C. (2014). Analysis of the hydrological response of a distributed physically-based model using post-assimilation (EnKF) diagnostics of streamflow and in situ soil moisture observations. *Journal of Hydrology*, *514*, 192–201. https://doi.org/10.1016/j.jhydrol.2014.03.072

Tshimanga, R. M., & Hughes, D. A. (2014). Basin-scale performance of a semidistributed rainfall-runoff model for hydrological predictions and water resources assessment of large rivers: The Congo River. *Water Resources Research*, *50*(2), 1174–1188. https://doi.org/10.1002/2013WR014310

Visweshwaran, R., Ramsankaran, R., & Eldho, T. I. (2024). Improving modelled streamflow using time-varying multivariate assimilation of remotely sensed soil moisture and *in-situ* streamflow observations. *Advances in Water Resources*, *186*, 104676. https://doi.org/10.1016/j.advwatres.2024.104676

Wagner, W., Verhoest, N. E. C., Ludwig, R., & Tedesco, M. (2009). Editorial and quot;Remote sensing in hydrological sciences& quot. *Hydrology and Earth System Sciences*, *13*(6), 813–817. https://doi.org/10.5194/hess-13-813-2009

Wahr, J., Swenson, S., & Velicogna, I. (2006). Accuracy of GRACE mass estimates. *Geophysical Research Letters*, *33*(6). https://doi.org/10.1029/2005GL025305

Wanders, N., Bierkens, M. F. P., de Jong, S. M., de Roo, A., & Karssenberg, D. (2014a). The benefits of using remotely sensed soil moisture in parameter identification of large-scale hydrological models. *Water Resources Research*, *50*(8), 6874–6891. https://doi.org/10.1002/2013WR014639

Wanders, N., Karssenberg, D., de Roo, A., de Jong, S. M., & Bierkens, M. F. P. (2014b). The suitability of remotely sensed soil moisture for improving operational flood forecasting. *Hydrology and Earth System Sciences*, *18*(6), 2343–2357. https://doi.org/10.5194/hess-18-2343-2014

Wang, W., Rong, Y., Zhang, C., Wang, C., & Huo, Z. (2024). Data assimilation of soil moisture and leaf area index effectively improves the simulation accuracy of water and carbon fluxes in coupled farmland hydrological model. *Agricultural Water Management*, *291*, 108646. https://doi.org/10.1016/j.agwat.2023.108646

Wang, X. Y., Li, X., Zhu, J., & Tanajura, C. A. S. (2018). The strengthening of Amazonian precipitation during the wet season driven by tropical sea surface temperature forcing. *Environmental Research Letters*, *13*(9), 094015. https://doi.org/10.1088/1748-9326/aadbb9

Wang, Y. (2004). Seasonal change in the extent of inundation on floodplains detected by JERS-1 Synthetic Aperture Radar data. *International Journal of Remote Sensing*, *25*(13), 2497–2508. https://doi.org/10.1080/01431160310001619562

Westerhoff, R. S., Kleuskens, M. P. H., Winsemius, H. C., Huizinga, H. J., Brakenridge, G. R., & Bishop, C. (2013). Automated global water mapping based on wide-swath orbital synthetic-aperture radar. *Hydrology and Earth System Sciences*, *17*(2), 651–663. https://doi.org/10.5194/hess-17-651-2013

White, L., Brisco, B., Pregitzer, M., Tedford, B., & Boychuk, L. (2014). RADARSAT-2 beam mode selection for surface water and flooded vegetation mapping. *Canadian Journal of Remote Sensing*, *40*(2), 135–151. https://doi.org/10.1080/07038992.2014.943393

Willmott, C. J., Robeson, S. M., & Feddema, J. J. (1994). Precipitation averages from rain-gauge networks. *International Journal of Climatology*, *14*(4), 403–414. https://doi.org/10.1002/joc.3370140405

Wongchuig, S., Cauduro Dias de Paiva, R., Biancamaria, S., & Collischonn, W. (2020). Assimilation of future SWOT-based river elevations, surface extent observations and discharge estimations into uncertain global hydrological models. *Journal of Hydrology*, *590*, 125473. https://doi.org/10.1016/j.jhydrol.2020.125473

Wongchuig, S., de Paiva, R. C. D., Siqueira, V., & Collischonn, W. (2019). Hydrological reanalysis across the 20th century: A case study of the Amazon Basin. *Journal of Hydrology*, *570*, 755–773. https://doi.org/10.1016/j.jhydrol.2019.01.025

Wongchuig, S., Fleischmann, A., Paiva, R., & Fadel, A. (2020). Towards discharge estimation for water resources management with a semi-distributed model and local ensemble Kalman filter data assimilation. *Journal of Hydrologic Engineering*, *26*(2), 05020047. https://doi.org/10.1061/(ASCE)HE.1943-5584.0002027

Wongchuig, S., Paiva, R., Espinoza, J. C., & Collischonn, W. (2017). Multi-decadal hydrological retrospective: Case study of Amazon floods and droughts. *Journal of Hydrology*, *549*, 667–684. https://doi.org/10.1016/j.jhydrol.2017.04.019

Yamazaki, D., de Almeida, G. A. M., & Bates, P. D. (2013). Improving computational efficiency in global river models by implementing the local inertial flow equation and a vector-based river network map. *Water Resources Research*, *49*(11), 7221–7235. https://doi.org/10.1002/wrcr.20552

Yamazaki, D., Ikeshima, D., Tawatari, R., Yamaguchi, T., O'Loughlin, F., Neal, J. C., et al. (2017). A high-accuracy map of global terrain elevations. *Geophysical Research Letters*, *44*(11), 5844–5853. https://doi.org/10.1002/2017GL072874

Yan, H., & Moradkhani, H. (2016). Combined assimilation of streamflow and satellite soil moisture with the particle filter and geostatistical modeling. *Advances in Water Resources*, *94*, 364–378. https://doi.org/10.1016/j.advwatres.2016.06.002

Yu, Z. (2015). Hydrology, floods and droughts | modeling and prediction. In *Encyclopedia of atmospheric sciences* (Vol. 3, pp. 217–223). Elsevier. https://doi.org/10.1016/B978-0-12-382225-3.00172-9

Zaitchik, B. F., Rodell, M., & Reichle, R. H. (2008). Assimilation of GRACE terrestrial water storage data into a land surface model: Results for the Mississippi River Basin. *Journal of Hydrometeorology*, *9*(3), 535–548. https://doi.org/10.1175/2007JHM951.1

Zhu, J., Zheng, F., & Li, X. (2011). A new localization implementation scheme for ensemble data assimilation of non-local observations. *Tellus A: Dynamic Meteorology and Oceanography*, *63*(2), 244–255. https://doi.org/10.1111/j.1600-0870.2010.00486.x

Zou, L., Zhan, C., Xia, J., Wang, T., & Gippel, C. J. (2017). Implementation of evapotranspiration data assimilation with catchment scale distributed hydrological model via an ensemble Kalman Filter. *Journal of Hydrology*, *549*, 685–702. https://doi.org/10.1016/j.jhydrol.2017.04.036